# Synergetic influence of beta-caryophyllene on wound healing

**(81 characters)**

**Short title: Beta-caryophyllene and wound healing**

[1*]Sachiko Koyama, [2]Anna Purk , [3]Manpreet Kaur, [4]Helena A. Soini, [4]Milos V. Novotny, [1]Keith Davis, [5]Cheng Kao, [6]Hiroaki Matsunami, [7]Anthony Mescher

Affiliations

[1]Department of Biology, Biotechnology Program, Indiana University, Bloomington, IN, USA.

[2]School of Public Health, Indiana University, Bloomington, IN, USA

[3]Department of Psychological and Brain Sciences, Indiana University, Bloomington, Indiana, USA

[4]Department of Chemistry, and Institute for Pheromone Research, Indiana University, Bloomington, Indiana, USA

[5]Department of Molecular and Cellular Biochemistry, Indiana University, Bloomington, Indiana, USA

[6]Department of Molecular Genetics and Microbiology, School of Medicine, Duke University, Durham, North Carolina, USA

[7]Department of Anatomy and Cell Biology, School of Medicine, Indiana University, Bloomington, Indiana, USA

* Correspondence author

E-mail: apodemusmice@gmail.com

# Abstract

Beta-caryophyllene, an odoriferous bicyclic sesquiterpene found in various herbs and spices, is a ligand of the cannabinoid receptor 2 (CB2). Activation of the CB2 will decrease pain and we hypothesized that beta-caryophyllene can affect wound healing. Here we show that mice cutaneous wounds treated with beta-caryophyllene had enhanced re-epithelialization. The treated tissue showed higher cell proliferation and cells treated with beta-caryophyllene showed higher cell migration, suggesting that the higher re-epithelialization is due to the enhanced cell proliferation and cell migration. The treated tissues also had up-regulated genes for hair follicle bulge stem cells. Olfactory receptors were not involved in the enhanced wound healing, and beta-caryophyllene also activated TRP channel genes. There were sex differences in the impact of beta- caryophyllene. Our study suggests that chemical compounds included in essential oil have the capability to improve wound healing, an effect generated by synergetic impacts of multiple pathways. (146 words)

# Introduction

Odors from other conspecific individuals [1] and in the environment [2-6] affect behaviors and physiological conditions. The significance of olfactory stimuli in our life tends to be underestimated. However, we have a long history of even utilizing odorants to impact our behaviors and physiological conditions. Various herbal plants' and spices' extracts have been used to reduce stress, pain, and to promote healing wounds [2-6]. In spite of such long history of using herbal extracts, there have been few examination on the functions of these extracts and little research on their mechanisms of action.

Olfactory receptors are expressed in both olfactory neurons and in non-olfactory tissues, such as skin and circulatory organs [7,8]. Furthermore, some odorants activate both olfactory receptors and non-olfactory receptors. Beta-caryophyllene (BCP), which is an odoriferous bicyclic sesquiterpene present in many herbs and spices, is a ligand of cannabinoid receptor 2 (CB2) [9] as well as the olfactory receptors. How odorants such as BCP act through distinct receptor classes is important for the most effective use of BCP.

The CB2 receptor is expressed in nerve cells, immune tissue, hair follicles, sebaceous glands, dermomuscular layer, and vascular smooth muscle in the intact skin [10]. Activation of CB2 improved re-epithelialization in wound healing [11,12]. Essential oils that contain BCP also improved wound healing [13], although it is not clear whether BCP had a direct or indirect role. In this project, we examined whether BCP can improve re-epithelialization and, if so, whether olfactory system is involved in the impact.

# Results and discussion

## BCP treatment enhanced re-epithelialization

Wound healing is a series of overlapping cellular and biochemical processes that restore the integrity of injured tissues. In general, healing occurs with four overlapping phases that takes place from minutes to weeks: hemostasis, inflammation, cell proliferation and migration, and maturation/scarring [14-17]. We examined whether exposure to BCP will affect cell proliferation and the re-epithelialization of mouse skin in a full thickness wound generated in mouse backs using scissors. The wound was then covered with a device that can retain either 50 uL of BCP (50mg/kgbw, diluted with olive oil) or a control (olive oil alone) (see Materials and Methods for details, S1 Fig). Throughout the study, none of the mice exhibited behaviors suggestive of irritation with the BCP (S2, S3 Fig). Immunofluorescence staining of keratin-14 (K14), a marker of re-epithelialization [18], revealed that wounds treated with BCP had increased keratinocyte migration distance from intact skin near the wound toward the wound center relative to the controls, indicating their improved re-epithelialization (Fig. 1). Staining for the proliferating cell nuclear antigen (PCNA) showed that many cells were proliferating at the wound edge in both BCP and Oil groups (green color in the wound edge area in Fig. 1b). In the BCP group, there were many PCNA+ fibroblast cells in the reticular dermis (lower area of dermis). The fibroblast cells in the reticular dermis migrate into the wound bed and form extracellular matrix of granulation tissue [19]. The results on K14 and PCNA show that BCP-treated group exhibit higher re-epithelialization and cell proliferation.

Another marker of re-epithelialization is the expression of filaggrin, a marker of differentiated skin [20]. Filaggrin is expressed in the upper layer of epidermis (stratum corneum) and functions as skin barrier, protecting the body from losing water and from

exogenous pathogens [20]. In the BCP-treated wounds, the range of differentiated stratum corneum layer in the invading epidermis was wider and the expansion from the wound edge was longer when compared to the Oil group (Fig. 2 red).

Estrogen is known to accelerate wound healing [21]. We examined if there are differences in the expression of estrogen receptor alpha by exposure to BCP. Estrogen receptor alpha was expressed strongly in the dermis fibroblasts of both BCP and Oil group without differences (Fig. 2). Platelet-derived growth factor-A and –B (PDGF-A and –B) are expressed in fibroblasts and keratinocytes [22]. PDGF receptors (PDGFR) are expressed in fibroblasts, smooth muscle cells, epithelial cells, macrophages, and their expression increases when there is inflammation [22]. In wound healing, PDGF stimulates mitogenesis and chemotaxis of fibroblasts, smooth muscle cells, neutrophils and macrophages, and stimulates production of fibronectin, collagen, proteoglycans and hyaluronic acid [22]. PDGFRα also has a role in extracellular matrix and hepatocyte growth factor production in fibroblasts in remodeling of connective tissue [23]. Immunofluorescence staining for PDGFRα showed that it is expressed strongly in the epidermis and the wound edge of the tissue treated with BCP (Fig. 2b). In the tissues treated with Oil, PDGFRa was expressed strongly only at the wound edge (Fig. 2b). Vimentin, which has a role in fibroblast proliferation and keratinocyte differentiation [24, 25], was expressed strongly in the wound edge (Fig. 2b red) of both the BCP-treated and Oil-treated wound. These results suggest that the impact of BCP is specifically strong on the invasion of epidermis and differentiation of keratinocytes, enhancing the re-epithelialization of the wounded area.

**Fig 1. Re-epithelialization measured by keratin 14. (a)** Immunofluorescence staining to K14 (red) and PCNA (green) with nucleus staining using Draq5 (blue) of skin with wound treated with BCP or with oil. **(b)** Higher magnification images of areas of boxes in **(a)**. PCNA was expressed in nucleus and, when density of cells increased, it became expressed in cytoplasm **(b)**. This was observed at the center of the wound. In: intact area, W: wounded area. **(c, d)** Length of K14+ staining area from the boundary of intact and wounded area to the center of the wound in skin harvested on post-surgery day 3 **(c)** and 4 **(d)**. Dots indicate each data and the height of bars indicates the median. Horizontal lines indicate quartiles. 3$^{rd}$ day, Kolmogorov-Smirnov test, $P$=0.008, BCP, n=20, Oil, n=15; 4$^{th}$ day, Kolmogorov-Smirnov test, $P$=0.002, *: $P$<0.05, BCP, n=16, Oil, n=16. (160 words)

**Fig. 2 Expression of filaggrin (red) and estrogen alpha (green) (a), and PDGFR (green) and vimentin (red) (b) in the wounded area of mice. (a)** View at the wound edge. In: intact area, WE: wound edge, WB: wound bed. Scale bar is in μm. Dotted lines show the boundaries between the intact area and wound edge, and the wound edge and wound bed. Filaggrin staining of BCP group was broader in width and longer in the distance from wound edge. Estrogen alpha staining did not show obvious differences between groups. **(b)** PDGFR expression in the epidermis was stronger in the BCP group. Both BCP and Oil group showed large area of staining of PDGFR in the wound edge (WE) and wound bed (WB). Vementin staining did not show obvious differences between BCP group and Oil group. In: intact area, WE: wound edge, WB: wound bed. Scale bars are in μum. (148 words)

## BCP treatment enhanced cell proliferation

To determine the rate and location of cell proliferation in the wounded tissue, 5-bromo-2'-deoxyuridine (BrdU) was injected twice every 2 hours and tissues were harvested 2 hours after the second injection (see Materials andMethods for details). Significantly more BrdU+ cells were found on the basal layer of the interfollicular epidermis and hair follicles, and in the papillary dermis [26-28] in the BCP-treated wounds. In both the BCP-treated and controls, there were many BrdU+ cells at the wound margin and wound bed (Fig. 3). Previous studies have shown that proliferation takes place at a proliferative hub, which is from 2 mm outside of wound edge until 3 mm from wound edge [29]. We observed that cell proliferation in the controls took place highly at the wound margin and at the basal layer of the interfollicular epidermis (Fig. 3f, Oil). In contrast, the BCP-treated wounds had higher cell proliferation in the interfollicular epidermis, in the dermis, at the hair follicles, and in the wound bed (Fig. 3f, BCP).

Stem cells in the hair follicle contributes to re-epithelialization by migrating from hair follicle bulge to epidermis and then to the center of the wound [30]. The strong BrdU staining of hair follicles in BCP-treated wounds compared to the controls suggest that a larger number of hair follicle stem cells may have contributed to the enhanced re-epithelialization in BCP group.

**Fig 3. BrdU+ cells in the epidermis and dermis. (a)** BrdU+ cells in the epidermis (epi in **(f)**) (Student T-test, T=3.077, df=8, P=0.015, BCP, n=5, Oil, n=5), **(b)** BrdU+ cells in the

wound margin (wm in **(f)**) (Student T-test, T=1.343, df=8, P=0.216, BCP, n=5, Oil, n=5), **(C)** BrdU+ cells at the hair follicle (h in **(f)**) (Student T-test, T= 3.038, df=8, P=0.015, BCP, n=5, Oil, n=5). **(d)** BrdU+ cells at the dermis excluding wound margin (Student T-test, T=4.645, df=8, P=0.002, BCP, n=5, Oil, n=5). **(e)** BrdU+ cells at the BrdU+ cells at the wound bed (Student T-test, T=2.197, df=8, P=0.059, BCP, n=5, Oil, n=5). **(f)** Representative views of combined photos used in quantification for each groups. h: hair follicle, epi: epidermis, der: dermis, wm: wound margin, wb: wound bed, scale bar: 200 μm. Numbers below and above the photos are operationally assigned numbers for explanation in the text on locations in the wound. Dotted lines show the boundaries between epidermis and dermis, dermis and wound margin zone, and wound margin zone and wound bed. (152 words)

If enhanced re-epithelialization was due to a reduction of inflammation and an early shift to the cell proliferation/migration stage, then BCP should not impact cultured cells. To test this hypothesis, we conducted time-lapse imaging for 7 hours and enumerated cell division. We conducted this with different concentrations of BCP. We found a peak of cell proliferation at 26 μM BCP, which decreased at higher concentrations (Fig. 4). In higher concentrations we observed These results suggested that BCP treatment was on cell proliferation and enhanced re-epithelialization rather than the suppression of inflammation.

**Fig 4. Proliferating primary fibroblast cells exposed to BCP at various concentration.** Number of dividing and apoptotic cells during 7 hours of exposure to BCP. (22 words)

## BCP enhanced cell migration

The increased cell migration by BCP was not reported previously and we want to examine this further. To determine whether exposure to BCP can stimulate cell migration, we conducted *in vitro* assays of scratch tests and chemotaxis assays. Primary cultured fibroblasts and keratinocytes from C57BL/6 mice exposed to BCP (diluted with DMSO) for 24 hours showed higher chemotactic responses relative to the controls (fibroblasts, 2.1 times higher numbers of cells, and keratinocytes, 2.5 times higher number of cells, both compared to control condition cells exposed to DMSO) (Fig. 5a, b, c). However, exposure to BCP did not stimulate chemotactic responses in fibroblasts isolated from CB2 knockout mice (1.2 times higher number of cells compared to control condition cells exposed to DMSO) (Fig. 5d). These results suggest that activation of CB2 could lead to an increase in cell migration.

**Fig 5. Influence of BCP on cell migration. (a)** Representative results of chemotaxis assay. Cells showed chemotactic responses to BCP. Fibroblasts and keratinocytes were exposed either to BCP or to DMSO (control) in culture media in chemotaxis assay kit. WT cells exposed to BCP showed significantly more chemotactic responses toward the bottom of the inserts (fibroblasts, Student T-test, T=2.564, df=8, P=0.033, BCP, n=4, DMSO, n=4, **(b)**; keratinocytes, Student T-test, T=2.456, df=8, P=0.04, BCP, n=4, DMSO, n=4, **(c)**), but cells isolated from CB2 knockout mice did not show differences between these exposed to BCP and these exposed to DMSO control (fibroblasts, Student T-test, T=0.944, df=4, P=0.398, BCP, n=3, DMSO, n=3, **(d)**). **(e, f, g)** Results of scratch tests. Representative images on the influence of BCP (27 μM) on cell migration of fibroblasts. Six hours after scratch **(e)** and 1

197 day after scratch **(f)**. Dotted white lines show the edge of scratched area. Scale bar = μm, **(g)**
198 The distance cells migrated during the 6 hours shown as comparison to the original width
199 (% of shrink in width). O% means no change from original width. ANOVA, Medium type,
200 $F_{1,8}$=7.16, P=0.028, cell type, $F_{1,8}$=0.365, P=0.562, BCP, n=3, DMSO, n=3. (178 words)
201
202 In the chemotaxis assay above we found that cells show chemotactic responses toward
203 BCP. We then conducted scratch tests to determine if exposure to BCP stimulates
204 chemotactic responses to repopulate in petri dishes. After culture dish reached to
205 confluent, the culture media was replaced to culture media containing containing BCP
206 (23μM/10 μL DMSO/10 mL cell culture media) or DMSO (10 μL/10mL cell culture media).
207 Exposure to BCP increased the cell migration to the scratched area about (39.2% decrease
208 in the width in 6 hours), relative to the control (6.7% decrease in the width in 6 hours).
209 Both the cells from CB2 knockout mice exposed to BCP also showed comparable rate of
210 repopulating the devoided area (34.0% decrease in the width in 6 hours) (Fig. 5e, f, g).
211 These results suggest that BCP can stimulate cell migration, but most likely through more
212 than one pathway.
213 We started this study with the hypothesis that BCP will positively impact wound
214 healing by activating signaling by the CB2. While BCP did improve re-epithelialization, the
215 results of the cell migration studies showed that BCP's effect on re-epithelialization may be
216 more complicated than through the activation of CB2. Therefore, we examined whether
217 CB2 antagonist and agonist will affect the re-epithelialization. AM630, an antagonist of CB2
218 [31] was daily injected 20 min before the daily application of BCP, CB2 agonist JWH133
219 [32] was topically applied instead of BCP to determine if it generates similar impact as BCP.

Then tissues of BCP group, Oil group, AMP630+BCP group, and JWH133 group were harvested on the 5$^{th}$ day post-surgery. Sections were stained with K14 and the distance of migration from the edge of the wound was measured. Consistent with our previous observations, topical application of BCP enhanced re-epithelialization. CB2 agonist, JWH133 significantly enhanced re-epithelialization compared to Oil group (Fig. 6). When CB2 antagonist AM630 was injected daily to mice treated with BCP, the results were not clear. Re-epithelialization was not statistically different from Oil group but the variance was large and there was tendency of differences (P=0.071) (Fig. 6). These results suggest that there could be some other pathways involved in the BCP enhanced re-epithelization of the wounds.

**Fig. 6. Re-epithelialization (K14+ distance from wound edge) in the mice exposed to BCP, Oil, CB2 agonist JWH133, and BCP+CB2 antagonist AM633**. **(a)** Length of K14+ staining area from the boundary of intact and wounded area to the center of the wound in skin harvested on post-surgery day 5 from mice exposed to BCP, oil, JWH133 or injected CB2 antagonist AM630 daily before daily treatment with BCP. Dots indicate each data and the height of bars indicates the median. Horizontal lines indicate quartiles. ANOVA, $F_{3,53}$=5.51, $P$=0.002) (ANOVA, $F_{3,53}$=5.51, $P$=0.002. Post-hoc pairwise analyses between BCP vs. oil, Tukey's post-hoc pairwise comparison, $P$=0.002, CB2 agonist JMW133 group vs. oil group, Tukey's post-hoc pairwise comparison, $P$=0.071, and CB2 antagonist AM630+BCP group vs. BCP group, Tukey's pairwise comparison, $P$=0.097; BCP, n=9, Oil, n=10, JWH133, n=8, AM630+BCP, n=7). (b) Representative images of JWH133 group and BCP+AM630 group. In: Intact area, W: wounded area. (146 words)

## BCP changes gene expression in the wounded skin

In order to better predict the pathways through which BCP acts, we conducted RNA sequencing and transcriptome analyses. The skin from mice 17 to 18 hours post-injury treated with BCP or oil were used. The transcriptome of mice that were not injured (NT group) were also analyzed to determine which up/down-regulations are caused by injury itself.

When comparison was made between BCP group vs. NT group and Oil group vs. NT group, the patterns of up/down-regulated genes of BCP group and Oil group were similar (38 out of 50 top significant genes were common). This suggests that these genes could be the genes that become up/down-regulated when there is skin injury (S5 Fig).

When comparison was made between BCP group vs. Oil group, significant differences in gene expressions between BCP group and Oil group were found (Fig 7). BCP-treatment significantly up-regulated a large number of genes, the 50 whose expression changed the most are in Table 1. Twenty % of the up-regulated genes codes for keratins (*Krt*) or keratin-associated proteins (*Krtap*) [33] (Table 1). Krtap genes are expressed in cells of the hair shaft cortex [34], where we had observed an increased number of BrdU+ cells (Fig. 3). Other than the possible role of it on enhancing re-epithelialization, this result also suggests the possibility that exposure to BCP promotes more complete skin regeneration and hair neogenesis. The remaining forty of the top 50 up-regulated genes codes for functions in cell migration (e.g. *Adamts*) [35], cell fate determination, and hair follicle formation (*Bambi, Msx2, Dlx3, Padi1, Hoxc13, S100a*) [36- 41]. These results overall suggest that BCP has impacts on hair follicle stem cell production and skin regeneration to aid in wound healing.

**Fig 7. Results of RNA sequencing of post-surgery 17 hours skin and intact skin.**

Heatmap showing the top 50 significant gene expressions in the skin exposed to BCP (n=2) or oil (n=3), 17 to 18 hours post-surgery (inflammation stage), and in the skin of mice without skin excision (NT group) (n=3). Comparison between BCP vs. oil **(a)** showed clear difference between BCP and oil. **(b)** Volcano plot from the comparison between BCP vs. oil. Y-axis shows log10 (p value) and X-axis shows log2 fold change value. (81 words)

**Table 1 Top 50 genes altered in mice treated with oil and BCP groups. Top 50 genes were all up-regulated in BCP group compared to Oil group.**

| Genes | Log2FC | Pvalue | Family/roles and functions | References |
|---|---|---|---|---|
| *Krtap3-1* | 8.355 | 1.43E-16 | Krtap family; keratin associated protein; | |
| *Krtap3-2* | 3.195 | 6.4E-19 | | |
| *Krtap3-3* | 5.357 | 3.6E-43 | | |
| *Krtap4-9* | 8.410 | 3.02E-13 | | |
| *Krtap16-1* | 9.052 | 8.86E-18 | | |
| *Krtap17-1* | 5.949 | 6E-25 | | |
| *Krt31* | 9.963 | 9.34E-18 | Krt family; keratin | |
| *K rt32* | 2.876 | 8.67E-17 | | |
| *Krt39* | 4.537 | 2.64E-14 | | |
| *Krt83* | 8.568 | 1.85E-14 | | |
| *Dok4* | 1.116 | 1.04E-16 | Dok family; docking protein; "Associate with receptor tyrosine kinase c-Ret and function in c-Ret-mediated neurite outgrowth"; "play a positive role in activation of the MAP kinase pathway" (Grim et al. 2001) | Grim et al. 2001 |
| *Dlx3* | 2.876 | 1.24E-20 | DLX family; distal-less homeobox; keratinocytes differentiation | Bhattacharya et al. 2017; Palazzo et al. 2017 |
| *Dlx4os* | 3.393 | 1.99E-15 | | |
| *Nkd2* | 1.739 | 5.68E-15 | Naked cuticle family; a major component of Wnt signaling; "negatively regulates canonical Wnt signaling by binding Dishevelled" (Dsh) (Li et al. 2004) | Li et al. 2004 |
| *Ephb3* | 0.964 | 6.41E-15 | Developmental process; embryogenesis | Flanagan and Vanderhaeghen 1998; Zhou 1998 |
| *Gabrp* | 2.536 | 5.91E-21 | | |
| Gpr37 | 2.350 | 4.81E-16 | | |

| | | | | |
|---|---|---|---|---|
| *Psors1c* | 3.526 | 3E-22 | An immune system gene related to develop psoriasis, a disfiguring inflammatory skin disease | |
| *Cpm* | 2.030 | 1.39E-13 | Machrophage differentiation | |
| *Pinlyp* | 3.894 | 1.67E-16 | | |
| *Csdc2* | 3.974 | 8.42E-22 | Hair follicle cycling | Yang et al. 2017 |
| *S100a7a* | 4.018 | 4.15E-21 | "functions as a transglutaminase substrate/cornified envelope precursor, signal transduction protein, chemokine, and antibacterial protein in normal epidermis" (Eckert and Lee, 2006); Inflammation and cell migration; chemotaxis | Eckert and Lee 2006; Zwicker et al. 2012; Batycka-Baran et al. 2015 |
| *Unc5b* | 1.067 | 1.95E-17 | Morphogenesis; Potential mediaters of beta-catenin signaing; angiogenesis | Lu et al. 2004; Zhang et al. 2008; |
| *Adamts18* | 4.300 | 4.28E-14 | Development, angiogenesis, coagulation | Wei et al. 2014; Kelwick et al 2015 |
| *Sptssb* | 4.234 | 8.74E-17 | Axon | Zhao et al. 2015 |
| *Gm10318* | 10.288 | 1.12E-15 | Nothing known so far | |
| *Otop2* | 5.273 | 4.2E-19 | | |
| *Tchhl1* | 10.815 | 1.37E-22 | Expressed in basal layer of epidermis; expressed in the nuclei of cultured growing keratinocytes | Yamakoshi et al. 2013 |
| *Vsig8* | 7.709 | 2.77E-18 | Hair shaft protein | Rice et al. 2011 |
| *Fam26d* | 10.723 | 2.77E-18 | | |
| *Ly6g6d* | 6.345 | 5.34E-25 | | |
| *Padi1* | 7.996 | 5.74E-14 | Epidermal differentiation | Chavanas et al. 2006; Moelants et al. 2013 |
| *Bambi* | 3.486 | 1.67E-26 | "Negatively regulates TGFbeta family signaling by a regulatory mechanism involving the interaction of signaling receptors with a pseudoreceptor" (Onichtchouk et al. 1999); mouse embryogenesis | Onichtchouk et al. 1999; Grotewold et al. 2001 |

| | | | | |
|---|---|---|---|---|
| *Tchh* | 7.708 | 2.17E-16 | Hair follicle inner root sheath | Yamamoto et al. 2009 |
| *Sytl2* | 1.916 | 3.27E-20 | Cellular activity | Fukuda and Mikoshiba 2001; Li et al. 2018 |
| *Bean1* | 3.567 | 7.9E-15 | | |
| *Zfp618* | 3.060 | 2.48E-14 | Development; cerebellar neural stem/progenitor cells during development | Naruse et al. 2018 |
| *Msx2* | 3.792 | 6.03E-20 | In epidermis, hair follicles and fibroblasts of developing fetal skin (Stelnicki et al 1997); in adult skin, confined to epithelial derived structures; hair cycle control and hair shaft differentiation (Kim and Yoon 2013) | Stelnicki et al. 1997; Kim and Yoon 2013) |
| *Rtkn2* | 3.410 | 7.44E-14 | | |
| *Lrrc75b* | 5.540 | 1.6E-18 | | |
| *Hoxc13* | 2.829 | 2.56E-13 | | |
| *Pm20d1* | 2.060 | 8.47E-15 | | |
| *Rhpn2* | 1.681 | 3.56E-13 | | |
| *D730001G18Rik* | 4.438 | 4.08E-48 | | |
| *Foxn1* | 1.368 | 3.81E-15 | | |
| *Car6* | 4.084 | 8.35E-33 | | |
| *Slc40a1* | 1.727 | 8.58E-21 | | |

Bhattacharya, S. J. et al. *Invest Dermatol*. **138**(5): 1052-1061 (2017).; Batycka-Baran, A. et al. *J Dermatol Sci*. **79**(3): 214-221 (2015).; Chavanas, S. et al. *J Dermatol Sci*. **44**(2): 63-72 (2006).; Eckert, R.L. & Lee, K.C. *J Invest Dermatol*. **126**(7): 1442-1444 (2006).; Flanagan, J.G., & Vanderhaeghen, P. *Annu Rev Neurosci*. **21**: 309-345 (1998).; Fukuda, M. & Mikoshiba, K. *Biochem Biophys Res Commun.* **281**(5): 1226-1233 (2001).; Grim, J. et al. *J Cell Biol*. **154**(2):345-354 (2001).; Grotewold, L. et al. *Mech Dev*. **100**(2): 327-330 (2001).; Kelwick, R. et al. *Genome*. **16**:113 (2015).; Kim, B.K. & Yoon, S.K. *J Dermatol Sci*. **71**(3): 203-209 (2013).; Li, C. et al. *PNAS* **101**(15): 5571-5576 (2004).; Li, X. et al. *Cell Tissue Bank*. **19**(3): 277-285 (2018).; Lu, X. et al. *Nature* **432**(7014): 179-186 (2004).; Moelants, E.A. et al. *Cytokines* **61**(1):161-167 (2013).; Naruse, M. et al. *Neurochem Res*. **43**(1): 205-211 (2018).; Onichtchouk, D. et al. *Nature* **401**(6752): 480-485 (1999).; Palazzo, E. et al. *Cell Death Differ*. **24**(4): 717-730 (2017).; Rice, R.H. et al. *J Invest Dermatol*. **131**(9): 1936-1938 (2011).; Stelnicki, E.J. et al. *Differentiation*. **62**(1): 33-41 (1997).; Wei, J. et al. *Front Biosci*. **19**:1456-1467 (2014).; Yamakoshi, T. et al. *Biochem Biophys Res Commun*. **432**(1): 66-72 (2013).; Yamamoto, S. et al. *Exp Dermatol*. **18**(2): 152-159 (2009).; Yang, M. et al. *Sci Rep*. **7**(1): 13502 (2017).; Zhang, Y. et al. *Development*. **135**(12).: 2161-2172 (2008).; Zhao, L. et al. *PNAS* **112**(42):12962-12967 (2015).; Zhou, R. *Pharmacol Ther*. **77**(3): 151-181 (1998).; Zwicker, S. et al. *Dtsch Med Wochenschr*. **137**(10): 491-494 (201

The transcriptome analysis prompted us to examine whether BCP treatment affected genes known as hair follicle stem cell markers [27]. The hair follicle bulge markers *Gli1*, *Lgr5*, and *Sox9* were significantly up-regulated (Log2FC, 2.4605, 1.236, 0.5377, respectively) in the BCP group compared to the Oil group (see bottom table in Fig. 8). Hair follicle infundibulum marker *Lrig1* was also significantly up-regulated by 40% (Fig. 8, log2FC 0.4035). These results on up-regulation of hair follicle bulge markers suggest that BCP treatment can stimulates hair follicle stem cell production.

**Fig 8. Comparison of the expression of hair follicle marker genes**. Hair follicle genes related to the bulge were significantly up-regulated in the mice exposed to BCP compared to Oil group. PValues show the results of comparison between BCP and Oil groups. *: P<0.05, **: P<0.01, ***: P<0.001. (31 words)

The inflammation stage of wound healing starts immediately after injury and pro-inflammatory cytokine levels usually peak within the first 10 to 20 hours [42,43], then decrease for 2 days. The main source of cytokines is known to be neutrophils [42]. In our study, we used 17 to 18 hours post-injury skin and, of the pro-inflammatory cytokines, IL-1β and IL6 genes were significantly down-regulated in the BCP group compared to Oil group (Table 2). This suggests that BCP treatment suppressed the acute inflammation after the skin exicision (Table 2). Studies have shown that there is a rebound in the inflammatory cytokines after 3 days, when fibroblasts migrate and new granulation tissues are formed, which suggest that the cytokines during the 'rebound' stage may play a role in wound *remodeling* [42]. Using the tissue harvested on post-surgery day 4, we examined the

expression of the pro-inflammatory cytokines IL-1β and TNFα (Fig. 9a and b). IL-1β expression was especially strong in the wound bed of the BCP-treated mice. IL-1β and TNFα were expressed 2.7 times higher and 2.0 times higher, respectively, at the wound bed in the BCP group when compared to the Oil group (compared using color intensity in the image field). Apoptosis is involved in various stages of the tissue repair with its main role in eliminating unwanted cells. If the acute inflammation immediately after injury is suppressed, it is possible to expect that apoptosis rate might be suppressed in BCP group. We conducted terminal deoxynucleotidyl transferase (TdT) dUTP nick-end labeling (TUNEL) assay to detect apoptotic cells. TUNEL+ cells were abundant in the wound bed of both BCP-treated and oil-treated wounds when compared to intact area. However, TUNEL staining was much stronger in the Oil-treated group (2.0 times higher in the color intensity in the Oil group compared to BCP group). In the BCP-treated wounds, TUNEL+ cells were present in the bottom of epidermis and dermis close to wound edge (Fig. 9c). These results suggest that, in the BCP group, pro-inflammatory cytokines are suppressed immediately following injury which may have produced reduced apoptosis at 4 days post-injury. And, although the expression of pro-inflammatory cytokines is suppressed in BCP group during the early stage after injured, they become more expressed than Oil group at post-surgery day 4, which is when they are at cell proliferation stage. The roles of these cytokines need to be addressed in future.

**Table 2. Expression of pro-inflammatory cytokines in BCP group compared to Oil group.**

| Gene | Log2FC | Pvalue |
|---|---|---|

| | | |
|---|---|---|
| *IL-1b* | -1.236 | 0.003 |
| *IL6* | -1.100 | 0.002 |
| *Tnf* | -0.571 | 0.052 |
| *Mmp8* | -2.06 | 9.00E-04 |
| *Mmp10* | -0.667 | 0.033 |
| *Mmp16* | -0.948 | 0.012 |
| *Mmp19* | -1.069 | 0.012 |
| *Mmp28* | -0.72 | 0.003 |
| *Casp4* | -0.691 | 1.10E-03 |
| *Casp8* | -0.508 | 5.17E-06 |
| *Casp14* | 0.76 | 0.001 |

**Fig. 9. IL-1β, TNFα in the skin at the wound bed and close to the wound, and TUNEL staining of the skin at the wound bed and close to the wound**. **(a)** IL-1β (red and purple) expression in the BCP and Oil group. Blue color as well as purple color is Draq 5+ cells. Green is autofluorescence. **(b)** TNFα expression (red and purple) expression in the BCP and Oil group. Blue color as well as purple color is Draq 5+ cells. Green is autofluorescence. **(c)** TUNEL staining with double staining with Draq 5. Green and light blue is TUNEL+ cells. Blue and light blue is Draq5+ cells. Scale bars are μm. (110 words)

CB1 gene expression was not significantly different between BCP and Oil group, whereas CB2 gene was, to our surprise, down-regulated in BCP group in the 17~18 hours post-injury skin. Recent studies have shown that TRP channels become activated by some phytochemicals [44]. We examined the expression of genes related to TRP channel and found that TRPM1, TRPM6, TRPV4, and TRPV6 were significantly up-regulated and TRPM2 and TRPM3 were significantly down-regulated in BCP group compared to Oil group (Table 3). Importantly, there are growing number of papers showing the roles of TRP channels in the initiation of pain and itch perception as well as epidermal homeostasis and hair follicle

regulation, making the TRP channels called the 'ionotropic cannabinoid receptors' [45]. Of the TRP channels called ionotropic cannabinoid receptors [45], the one that overlap with the TRP channel showing significant change after exposure to BCP was TRPV4, which showed significant up-regulation. TRPV4 is expressed in various cell types including sensory neurons and is considered to be a mechano/osmosensitive channel [46]. The results of our study and recent studies on the roles of TRP channels suggest that TRP channels could be involved in the enhanced re-epithelialization by BCP.

**Table 3. Expression of cannabinoid receptors and TRP channel genes.** Genes up-regulated in BCP group compared to Oil group are written in red color and down-regulated genes are written in blue color. Genes written black are not significantly different between BCP and Oil group. Genes written in bold letter have P values over E-5. NA in PValue is outlayer compared to other genes presumably because of its extremely high expression in BCP group compared to Oil group.

| Gene | Log2FC | Pvalue | |
|---|---|---|---|
| *CB1 (cnr1)* | -0.463 | 0.641 | |
| *CB2 (cnr2)* | -0.755 | 0.028 | pain, inflammation |
| *TRPA* | not found | | |
| *TRPC1* | 0.023 | 0.932 | |
| *TRPC2* | 0.350 | 0.326 | |
| *TRPC3* | -0.047 | 0.937 | |
| *TRPC4* | -0.083 | 0.861 | |
| *TRPC6* | -0.157 | 0.824 | |
| ***TRPM1*** | 4.156 | NA | melanin synthesis |
| *TRPM2* | -1.530 | 0.006 | cutaneous pain sensation |
| *TRPM3* | -0.902 | 0.047 | |
| *TRPM4* | 0.130 | 0.370 | |
| *TRPM6* | 0.604 | 0.004 | magnesium transport |
| *TRPM7* | -0.041 | 0.818 | |
| *TRPM8* | 2.582 | 0.427 | |
| *TRPV1* | -0.236 | 0.635 | |

| | | | |
|---|---|---|---|
| *TRPV2* | -0.391 | 0.125 | |
| *TRPV3* | 0.171 | 0.452 | |
| | | | interacts with beta-catenin |
| *TRPV4* | 0.586 | 0.008 | |
| ***TRPV6*** | 1.527 | 3.00E-10 | calcium absorption |
| | | | calcium dependent cell proliferation |
| | | | inhibition of apoptosis |

Ingenuity pathway analysis® (IPA®) was performed using the gene expression results. In the comparison of BCP vs. Oil group, signaling pathways related to inflammation and immune system (TREM1 signaling) [47] were suppressed in the BCP group (S6 Fig.). In addition, genes that encode functions for cell proliferation and migration (e.g. the sonic hedgehog pathway, the planar cell polarity, the signaling pathway, fibroblast growth factor signaling pathway, and Wnt beta-catenin signaling pathway [S7 Fig. a, b, c, d]) were activated compared to the Oil group. Table 4 summarizes the genes in these signaling pathways that became significantly up/down-regulated in the BCP group compared to Oil group. In each of these pathways, there were genes whose expression were dramatically increased (bold in Table 4). These could be the core genes affected by BCP: hedgehog interacting protein gene (*hhip*), sonic hedgehog gene (*shh*), and dual specificity protein phosphatase CDC14a (*cdc14a*) in sonic hedgehog signaling pathway [48], frizzled-5 (*fzd5*), wingless-type MMTV integration site family member 5a, 10b, 11 (*wnt5a, 10b, 11*) in planar cell polarity signaling pathway [49], fibroblast growth factor 22 and 23 (*fgf22, fgf23*) and phosphoinositide-3-kinase regulatory subunit 3 (*pik3r3*) in fibroblast growth factor signaling pathway [50}, and *wnt5a, 10b, 11*, whitefly-induced tomato gene (*wfi1*), transcription factor sox4 (*sox4*), and lymphoid enhancer-binding factor 1 (*lef1*) in

Wnt/beta-catenin signaling pathway [51]. Studies have found that, in case of adult skin, the hedgehog signaling is involved in epidermal homeostasis, *i.e.*, the hair cycle and regrowth of hair [52]. *GLI1* is expressed in hair follicle bulge and sonic hedgehog secreted from sensory neurons surrounding hair follicle bulge stimulates the Gli1+ cells in the upper region of the bulge to convert to multipotent stem cells and contribute to wound healing by becoming epidermal stem cells [53]. The planar cell polarity pathway is known to be involved in the collective and directed cell movements during skin wound repair [54-57] and coordinating the directions of cell migration [56]. Studies using transgenic mice have shown that the role of fibroblast growth factor signaling includes keratinocyte proliferation [57]. Overall, the results on gene expression in our study suggest that the exposure to BCP activated the pathways in a way to enhance 1) conversion of hair follicle bulge stem cells to epidermal stem cells, 2) keratinocyte cell proliferation, 3) coordinated and directed cell movement, which may have contributed to the enhanced re-epithelialization by exposure to BCP.

**Table 4. Significantly up/down-regulated genes in *shh, pcp, fgf, and wnt/beta-catenin* signaling pathways after exposure to BCP.** Genes with log fold change over 1 are shown. Up-regulated genes are written in red, and down-regulated genes are written in blue. Results of genes with over E-05 Pvalues are shown in bold letters. NA in PValues is outlayer compared to other genes presumably because of its extremely high expression in BCP group compared to Oil group.

| Pathway | ***Gene*** | **Log2FC** | **PValue** |
|---|---|---|---|
| sonic hedgehog | *Hhip* | 3.202 | 3.44E-06 |
| | *Ptch1* | 1.564 | 1.02E-04 |
| | *Ptch2* | 3.374 | 2.02E-04 |

| | | | |
|---|---|---|---|
| | *Shh* | 5.995 | NA |
| | *Gli1* | 2.46 | 1.76E-05 |
| | *Gli2* | 1.179 | 1.00E-03 |
| planar cell polarity | *Fzd5* | 1.086 | 7.48E-08 |
| | *Ror2* | 1.627 | 5.40E-05 |
| | *Wnt5a* | 1.606 | 7.84E-10 |
| | *Wnt10b* | 1.613 | 1.58E-08 |
| | *Wnt11* | 1.997 | 6.53E-11 |
| | *Ndp* | 1.2746 | 1.84E-02 |
| fibroblast growth factor | *Fgf5* | 2.109 | 2.40E-05 |
| | *Fgf22* | 1.292 | 1.49E-08 |
| | *Fgf23* | -1.809 | 1.97E-11 |
| | *Tlr9* | -1.953 | 3.60E-04 |
| | *Pik3R3* | 1.081 | 1.77E-06 |
| Wnt beta-catenin | *Wnt5a* | 1.606 | 7.84E-10 |
| | *Wnt10b* | 1.613 | 1.58E-08 |
| | *Wnt11* | 1.997 | 6.53E-11 |
| | *Wfi1* | 1.778 | 4.18E-09 |
| | *Sox4* | 1.662 | 1.12E-10 |
| | *Sox5* | 1.821 | 4.81E-05 |
| | *Sox13* | 1.406 | 9.10E-04 |
| | *Lef1* | 3.152 | 2.48E-10 |

## Sex differences in the impact of BCP

These results so far are based on experiments using female mice. Previous studies have shown sex differences in the morphology and physiology of mouse skin, with female mice having 40% thicker epidermis than males [58]. In addition, androgen receptors have inhibitory influence on wound healing in males [59], which may hinder the impact of BCP.

We tested whether the influences of BCP on wound healing in male mice is similar to its influences in females and found no statistically significant differences in re-epithelialization between BCP and Oil groups in males (based on K14 staining) (Fig 10). Whether males

need higher concentration of BCP to induce its impact or whether BCP does not affect males at all need to be addressed in future.

Sex steroids are known to affect wound healing [60], androgen receptor inhibiting wound healing [59] whereas estrogen accelerates it [21]. The re-epithelialization in Oil control group males was similar to that of the Oil group of female mice (Fig 10), which suggests that sex hormones did not suppress re-epithelialization in males.

**Fig 10. Influence of BCP on re-epithelialization in male and female mice.** Length of K14+ staining area from the boundary of intact and wounded area to the center of the wound in skin harvested on post-surgery day 4 from mice exposed to BCP or oil. Bar indicates median and line indicates 25 and 75% quartile. ANOVA, BCP vs. oil, $F_{1,66}$=14.793, $P$<0.001; gender, $F_{1,66}$=30.761, Tukey's post-hoc test, ***: P<0.001; females, BCP, n=16, oil, n=16, males, BCP, n=23, oil, n=15 (76 words)

## Olfactory receptors are not involved

BCP is an odorant. When mice are topically treated with BCP, they are exposed to its smell and there is a possibility that olfactory system has some role in the BCP mediated enhanced re-epithelialization. In addition, olfactory receptors are expressed in non-olfactory tissues. A synthetic analogue of sandalwood odorant, sandalore, is the ligand of olfactory receptor gene OR2AT4 and that OR2AT4 receptors are expressed in human skin [61]. Thus odorants can directly produce impact on non-olfactory tissues like the skin tissues [61] other than through the route of olfactory system to the brain, affecting the

emotional status [62]. There is a possibility that the impact of BCP was mediated by olfactory receptors expressed in the skin.

To examine if olfactory system and/or olfactory receptors expressed in skin has some role in the enhanced re-epithelialization by exposure to BCP, we conducted multiple experiments. First we tested if mice can smell BCP by testing the expression of immediate early gene protein in the olfactory bulb exposure to BCP and found clear expression of cfos protein, suggesting that it is highly likely that mice can smell BCP (S8 Fig.). Then we tested whether exposure to BCP only through air would produce similar impact as topical application, and found no improved re-epithelialization (S9 Fig ). It was clear that olfactory system was not involved in the impact of BCP on re-epithelialization.

To examine if olfactory receptors expressed in non-olfactory system are involved, we first examined the olfactory epithelium after exposure of mice to BCP for one hour to identify the olfactory receptor genes for BCP using pS6-IP RNAseq [63]. We could narrow down the candidates of olfactory receptor genes for BCP (S2 Table). It is known that odorants stimulate limited number of types of olfactory receptors [64,65]. As the BCP we used was not 100% in purity, multiple olfactory receptor genes were up-regulated following the exposure to BCP with *Olfr340* showing largest folder change and P-value (S2 Table). After this step, we went through the results of RNA sequencing of the skin to determine if the olfactory receptor genes up-regulated in olfactory epithelium by exposure to BCP are expressed in skin and are up-regulated after topical application of BCP. There were many olfactory receptor genes expressed in the skin (S3 Table), and one of them overlapped with the olfactory receptor genes up-regulated in olfactory epithelium (*Olfr111*), but none of them were up-regulated specifically in BCP group. From these

results, we conclude that olfactory receptors expressed in skin are not involved in the enhanced re-epithelialization by exposure to BCP.

## Synergetic influences by exposure to BCP

Wound healing starts from the inflammatory stage and shifts to cell proliferation stage. Since BCP is angonist of CB2 , we had assumed that it can improve wound healing by decreasing pain and reduce proinflammatory signals and speed up the shift to cell proliferation stage. However, our results suggests that BCP may directly impact cell proliferation and cell migration. BCP also stimulates mitogenesis of hair follicle stem cells. Hair follicle stem cells participate in re-epithelialization when there is cutaneous wound [30, 40], our study suggests that the enhanced re-epithelialization by exposure to BCP is mediated by BCP stimulated production of hair follicle stem cells in the bulge, and their migration to epidermis and to wound bed.

BCP is known to suppress apoptosis [66] and necroptosis [67], raising the possibility that their suppression enabled higher cells survival and proliferation. The suppression of *Septin4* (*Sept4*) has been shown to protect cells from cell death and promotes wound healing [68], however, *Sept4* was not up-regulated in our study and seemed to be not involved in the BCP enhanced re-epithelialization. It is possible that the exposure to BCP generates specific wound healing environment by up-regulating the genes related to embryonic growth as was suggested from our results on transcriptome analyses.

Our study focused on the early stage following skin excision. Studies have shown that oxidants from inflammatory cells are involved in fibrotic healing (scarring) [69,70], which suggests that suppression of inflammation through activation of CB2 by BCP, in addition to

up-regulation of genes related to embryonic growth would have high possibility of reducing scar formation. These possibilities need to be addressed in future by testing the influence of exposure to BCP on the late stage after injury.

## Odors affect us more than we think

It has been several decades since the first report that olfactory receptors are expressed in non-olfactory regions [71] and that odors have functions other than olfactory and pheromonal communication [72]. Our observations that BCP activates multiple types of receptors in the skin further unveils the complexity of chemical signaling. Although we humans typically rely on visual and auditory stimuli in communication, it is important to understand how odors in the environment, whether it is from other individuals [1] or from plants [2-6], could be affecting our conditions. In addition, BCP is but one component commonly found in essential oils of herbal extracts. Further examination of the compounds in herbal extracts could lead to additional useful molecules that could benefit our health.

# Materials and methods

## Mice strains

We used a standard murine model for wound healing. Mice were used between 8 to 10 weeks in age in *in vivo* experiments. C57BL/6J, and CB2-/- mice were used in experiments. Primary cells for *in vitro* experiments were obtained from P0 to P1 neonate pups or adult mice from C57BL/6J, or CB2-/- mice. In *in vivo* experiments, C57BL/6J mice were used. All

mice were kept at 14:10, L/D light cycle, and water and food were provided ad libitum. All the procedures were following protocols approved by the Indiana University Institutional Animal Care and Use Committee (IACUC).

## Surgery

We studied small full-thickness excisions on the backs of adult mice and developed methods to hold the treatment buffer solution on the wounded area (S1 Fig a). Hair of the dorsal area was removed and the area for surgery was cleansed using betadine and 70% ethanol. A small piece of dorsal skin of mice was excised (< 5mm x 5mm) under anesthesia. A silicone ring was attached to the wounded area using a liquid sealing bandage (S1 Fig a center) (OD: 15mm, ID: 8mm, thickness, 3mm). This ring served as a reservoir and 50 μL of BCP (50 mg/kgbw; 0.2nM) (W225207, Sigma-Aldrich, Co. St. Louis, MO) diluted in olive oil, or olive oil as control (O1514, Sigma-Aldrich, Co. St. Louis, MO), was placed in the reservoir. The gas chromatography-mass spectrometry (GC/MS) analysis of the BCP standard showed that it contained 81.8% BCP and 14.0% α-caryophyllene (α-humulene). The remaining 4.2% consisted of 1.6% caryophyllene oxide and minor amounts of other molecular weight 204 sesquiterpenes (0.1-0.8% each) (S4 Fig., S1 Table). Molecular weights are calculated by the amount of BCP (81.9% of the volume converted to molecular weight).

The ring was covered with PDMS (polydimethylsiloxane) (Dow Corning Sylgard® 184 Silicone Elastomer Kit; Dow Corning, Auburn MI) and sealed with liquid bandage to hold the BCP media or olive oil. A gauze bandage was used to loosely cover the body to prevent the mouse from removing the ring with PDMS lid (S1 Fig 1a, right down). The bandage and buffer media were removed daily and replaced with new bandage and buffer media. The

wounded area was collected on the 3rd, 4th, 5th day, and immediately fixed with 10% formalin for one day, then soaked in 70% ethanol.

## Gas chromatography – mass spectrometry (GC/MS) analysis of BCP

BCP was diluted to 180 ng/µL with tert-butyl methyl ether solvent (99+%, Aldrich Chemical Company, Milwaukee, WI). The BCP composition was analyzed using 2 µL of the diluted BCP in the thermal desorption tube of the Thermal Desorption Autosampler and Cooled Injection System (TDSA-CIS 4 from Gerstel GmbH, Mülheim an der Ruhr, Germany) connected to an Agilent6890N Gas chromatograph – 5973iMSD Mass spectrometer (Agilent Technologies, Inc., Wilmington, DE). BCP components were identified with spectra through NIST Mass Spectral Search Program for the NIST/EPA/NIH Mass Spectral Library (Version 2.0 a, 2002). Additionally, the mass spectra and Kovats retention index matches were verified with the reference spectra from Adam (2001) [73]. Caryophyllene oxide was verified with the standard (99%) from Sigma-Aldrich (St. Louis, MO).

## CB2 agonist and antagonist treatment

CB2 agonist JWH133 (1 µM; Cat. 10005428, Cayman Chemical Co., Ann Arbor, MI), dissolved in alcohol and kept at -20°C, was dissolved in olive oil after alcohol was evaporated and used instead of BCP in the daily treatment on the wounded area. CB2 antagonist, AM630 (4 mg/kgbw (7.9 µM/kgbw); SML0327, Sigma-Aldrich Corp. St. Louis, MO) was dissolved in saline and injected 20 min before the daily treatment of BCP.

## Immunofluorescence staining to evaluate re-epithelialization

Mice were euthanized by cervical dislocation and the wounded area was harvested, fixed in 10% formalin and then in 70% ethanol until embedded in paraffin. Samples were sectioned at 10 μm, deparaffinized and hydrated, went through antigen retrieval using sodium citrate buffer (10mM, >95°C for 20 to 30 min), blocked with 10% NGS, and primary stained (see below for antibodies) overnight at 4°C. Then sections were washed, secondary stained, nucleus stained using Draq 5, washed (3 times), and covered with Prolong Diamond (ProLong™ Diamond Antifade Mountant P36965, Thermo Fisher Scientific).

Antibodies used are as follows: proliferating cell nucleus antigen (PCNA (PC10) mouse mAb #2586, Cell Signaling Technology, Danvers, MA, 1:1000), keratin 14 (K14, rabbit pAb, 905301, 1:1000, BioLegend, San Diego, CA), PDGFRalpha (mouse mAb, sc-398206, Santa Cruz Biotechnology, CA, 1:1000), vimentin (rabbit, 10366-1-AP, Protein Tech, 1:500), estrogen receptor alpha (Eralpha, mouse mAb, sc-51857, sc-8002, Santa Cruz Biotechnology, 1:250), filaggrin (rabbit pAb, BioLegend, San Diego, CA, 1:1000), TNFalpha (rabbit pAb, ab6671, Abcam, 1:100), IL-1beta (rabbit pAb, ab9722, Abcam, 1:100). Alexa fluor 594 anti-rabbit and Alexa fluor 488 anti-mouse (both Invitrogen, 1:500). Stained sections were observed using laser scanning confocal microscope Leica SP5 at the IUB Light Microscope Imaging Center.

## TUNEL staining

Mice were euthanized by cervical dislocation and the wounded area was harvested, fixed in 10% formalin and then in 70% ethanol until embedded in paraffin. Samples were

sectioned at 10 μm, deparaffinized and hydrated. TUNEL staining was conducted following manufacturer's protocol (In Situ Cell Death Detection Kit, Version 17, Roche Diagnistics GmbH, Mannheim, Germany). Briefly, slide glasses were first rinsed with PBS for 5 min twice, then went through antigen retrieval using sodium citrate buffer (10mM, >95°C for 20 to 30 min), and rinsed with PBS for 10 min three times. Blocked with 0.1 M Tris-HCl, pH7.5 with 3% BSA and 20% normal bovine serum for 30 min. Slides were rinsed twice with PBS for 10 min twice. Then TUNEL reaction mixture were added and slides were incubated for 1 hour at 37C. Slides were rinsed for 10 min once, stained with Draq5 for 10 min at room temperature, and rinsed for 10 min three times. Finally, covered with Prolong Diamond (ProLong™ Diamond Antifade Mountant P36965, Thermo Fisher Scientific). Stained sections were observed using laser scanning confocal microscope Leica SP5 at the IUB Light Microscope Imaging Center.

## BrdU injection and staining

On post-surgery day 4, mice were injected with bromodeoxyuridine (BrdU) (300 mg/kgbw) twice every 2 hours, and the skin was harvested 2 hours after the second injection. Harvested skin was fixed with 10% formalin, and then with 70% ethanol on the following day. Samples were embedded in paraffin and cut into sections using microtome at 10 μm. Sections were then deparaffinized and hydrated, went through antigen retrieval using 4N HCl at 37°C for 30 min, washed with 0.1M PBS, blocked with 10% NGS, and went through overnight staining at 4°C with anti-BrdU (1:300, rat, Accurate Chemical Co. #OBT0030). On the second day, sections were washed with 0.1M PBS, stained with anti-rat Alexa fluor 488 (1:500, Invitrogen) at room temperature, washed, stained with Draq5,

washed, and covered after placing one drop of Prolong Diamond (ProLong™ Diamond Antifade Mountant P36965, Thermo Fisher Scientific). Sections were observed using laser scanning confocal microscope (Leica DMI 6000 CS inverted microscope) in the IUB Light Microscope Imaging Center and analyzed using Fiji/ImageJ software.

## Immediate Early Gene protein expression (c-*fos*) experiment and staining

Each mouse was exposed to BCP or male murine pheromone 2-sec-butyl-4,5-dihydrothiazole (SBT) (250ppm, positive control) [74,75] for 1 hour in a clean cage. Then mice were anesthetized with 2.5% isoflurane and cardiac perfused with saline for 2 min, followed by 4% paraformaldehyde for 6 to 7 min. The brains were dissected out and post-fixed with 4% paraformaldehyde overnight at 4 °C, transferred to PBS with 15% sucrose and kept at 4 °C. The brains were embedded in OCT on dry ice and cryosectioned using Leica CM1850 at 20 μm and kept at -20 °C until use.

For the staining of c-*fos* gene protein, the brain sections were washed 3 times for 10 mins with 0.1M PBS, blocked with 10% NGS, 0.5% Triton X-100 in 0.1M PBS for 1 to 2 hours, and went through primary staining with anti-c*fos* (Invitrogen OSR00004w, rabbit, 1:250; Abcam ab190289, rabbit, 1:2000) overnight at 4 °C. Then sections were washed 3 times for 10 mins and went through secondary staining (Alexafluor 594, anti-rabbit, 1:500), washed with 0.1M PBS, stained with Draq5, washed (0.1M PBS 3 times each 10 mins), and covered with Prolong Diamond. Bregma distance about 4.28mm was used in the comparison. The stained sections were observed using laser scanning confocal microscope

Leica SP5 at the IUB Light Microscope Imaging Center. Numbers of cfos+ cells in the whole glomerular layer, external plexiform layer, mitral layer, internal plexiform layer, and granule cell layer of olfactory bulb were counted using Fiji/Image J.

## Isolation of primary cells

Fibroblast isolation: Mice (neonate or adult) were euthanized by cervical dislocation and cleansed. Harvested skin was treated with 0.25% trypsin (Gibco, 15050065, Waltham MA) at 4°C overnight.

Dermis was collected after trypsin treatment, minced and pipetted to dissociate, and incubated at 37°C with collagenase A buffer in cell culture media (1 mg/mL). Following the incubation, the buffer with dissociated cells was filtered using 100 µL strainer, and centrifuged at 500 X G for 8 min. Supernatant was removed and the pellet was re-suspended in either CnT-PR-F media (CELLnTECH; Zen-Bio, Research Triangle Park, NC), filtered with 40 µm strainer, and centrifuged again at 500 X G for 8 min. Following another re-suspension to new culture media, cells were seeded to petri dishes to culture at 37°C with 5% $CO_2$.

Keratinocytes: Skin was collected from neonate mice after the mice were decapitated and cleansed. Collected skin was placed in petri dish with 0.25% Trypsin (Gibco, 15050065, Waltham MA) with its epidermis side up and above buffer and placed at 4°C for 6 to 8 hours. Then the epidermis of the skin was removed from dermis, minced and pipetted to dissociate in the trypsin buffer, filtered using 70 or 100 µm strainer, and centrifuged at 500 X G or 800G for 8 min. Supernatant was removed and the pellet was re-suspended in high calcium DMEM medium ((Gibco, 10569-010, Waltham MA) supplemented with FBS (10%),

p/s, and Glutamax), filtered using 40 µm, centrifuged again and resuspended with the high calcium DMEM medium. Then cells were seeded on Collagenase I coated petri dishes (Collagen I, Coated Plate 6 Well, Gibco Life technologies A11428-01, Waltham MA), incubated at 32 to 35°C[45] with 5% $CO_2$ with high calcium DMEM medium overnight[46]. On the following day, culture medium was replaced with low calcium medium (CnT-PR, CELLnTECH; Zen-Bio, Research Triangle Park, NC) and penicillin streptomycin (1140122, ThermoFisher Scientific, Waltham MA).

## Chemotaxis assay and scratch tests

Chemotaxis assay: Primary cultured cells (300 µL) were seeded in the inserts of 24 well cell migration plate (Cell Biolabs Inc, CBA100, CytoSelect 24 well cell migration assay kit) with 500 µL of DMEM cell culture media containing BCP (5 µL in 10 µL of DMSO in 10mL of cell culture media) or DMSO (control; 10 µL of DMSO in 10 mL of cell culture media) in the well, and incubated at 37°C and 5% $CO_2$ for 1 day (approximately 18 to 24 hours). Then the inserts were washed with water and observed under microscope, photographed using EVOS XL Core (ThermoFisher Scientific, Waltham MA), and the number of cells on the outside bottom of the insert was counted using Fiji/ImageJ.

Scracth tests: Primary cultured cells were seeded in 12 well plates. Two days later the culture media was changed to either 2 mL of DMEM cell culture media containing BCP (0.06 µL in 10 µL of DMSO in 10 mL of cell culture media) or DMSO (control; 10 µL of DMSO in 10 mL of cell culture media) and surface of the bottom of the wells was scratched with the thin side tips of 1mL pipet tips. Photos were taken immediately after the scratches

were made, 6 hours later and 1 day later. Widths of the scratch line were measured using Fiji/Image J.

## Time lapse *in vitro* observation of cell proliferation

Primary cultured cells were exposed to BCP in DMEM culture media or DMSO (control) in DMEM culture media on the next day after the cells were seeded on petri dishes with cover glass bottom (12-567-401, Thermo Scientific™ Nunc™). Immediately after the media was changed to a media with BCP or DMSO alone, cells were cultured on an Olympus OSR Spinning Disk Confocal microscope with Tokai Hit Stage Top Incubation system kept at 37°C and 5% $CO_2$. DIC images were taken every 3 mins for 7 hours using a Hammamatsu Flash 4V2 camera and movies were generated using Metamorph software. Obtained images were played and the number of dividing cells were counted.

## Transcriptome analyses using skin

The wounded part of skin was exposed to BCP or olive oil (control) and tissues were harvested 17 hours later based on the study which reported the time course in the expression of genes related to inflammatory responses [43]. Tissue from another group of mice was harvested similarly without wound (no-injury control). The wounded area and its surrounding area (2 x 2 cm) were immediately dissected out and RNA extraction was conducted using Maxwell® RSC simplyRNA Tissue Kit (AS1340, Promega, Madison WI) following manufacturer's protocol. The volume of extracted RNA was measured using Epoch™ Microplate Spectrophotometer (BioTek, Winooski, VT) with Take 3 Micro-Volume Plates (BioTek, Winooski, VT) and Gen5 Microplate Reader and Imager Software (BioTek,

Winooski, VT). The integrity was analyzed with Agilent Technologies 2200 Tape Station (Agilent Technologies). Input was quantified by using Qubit RNA BR Assay Kit and RNA-seq was conducted using NextSeq Series RNA-seq Solution, (Illumina) at the Center of Genomics and Bioinformatics, IUB. Samples were prepared using TruSeq Stranded mRNA HT Sample Prep Kit (Illumina). Sequencing was performed using an Illumina NextSeq 500/550 Kits v2 reagents with 75 bp sequencing module generating 43 bp paired-end reads. After the sequencing run, demultiplexing with performed with bcl2fastq v2.20.0.422.

## pS6-IP RNA-Seq analyses using olfactory epithelium

To perform pS6-IP RNA-Seq we used 4 pairs of litter-matched mice. We used both male and female mice in both control and experimental conditions with no specific orientation. Single pairs of mice were habituated in clean paper tubs in a fume hood for 1 hour. Following habituation, mice were transferred to another paper tub with a uni-cassette containing a 2 cm x 2 cm filter paper spotted with either water (control) or 1% (v/v) 10 L BCP dissolved in water (experimental) for 1 hour.

Following odor stimulation, mice were killed and the OE was dissected in 25 mL of dissection buffer (1× HBSS [Gibco, with $Ca^{2+}$ and $Mg^{2+}$], 2.5 mM HEPES [pH 7.4], 35 mM glucose, 100 µg/mL cycloheximide, 5 mM sodium fluoride, 1 mM sodium orthovanadate, 1 mM sodium pyrophosphate, 1 mM beta-glycerophosphate) on ice.

The dissected OE was transferred to 1.35 mL of homogenization buffer (150 mM KCl, 5 mM $MgCl_2$, 10 mM HEPES [pH 7.4], 100 nM Calyculin A, 2 mM DTT, 100 U/mL RNasin (Promega), 100 µg/mL cycloheximide, 5 mM sodium fluoride, 1 mM sodium orthovanadate, 1 mM sodium pyrophosphate, 1 mM beta-glycerophosphate, protease inhibitor (Roche, 1

tablet per 10 ml)) and homogenized three times at 250 rpm and nine times at 750 rpm (Glas-Col). The homogenate was transferred to a 1.5 mL lobind tube (Eppendorf), and centrifuged at 2,000 X G for 10 min at 4°C. The supernatant was then transferred to a new 1.5 mL lobind tube, to which 90 µL 10% NP-40 (vol/vol) and 70 µL 300 mM DHPC (Avanti Polar Lipids) were added. The mixture was centrifuged at 17,000 X G for 10 min at 4°C. The supernatant was transferred to a new 1.5 mL lobind tube and mixed with 6 µL pS6 antibody (Cell Signaling, D68F8). Antibody binding was allowed by incubating the mixture for 1.5 hour at 4°C with rotation. During antibody binding, Protein A Dynabeads (Invitrogen, 100 µL per sample) was washed three times with 900 µL beads wash buffer 1 (150 mM KCl, 5 mM $MgCl_2$, 10 mM HEPES [pH 7.4], 0.05% BSA (wt/vol), 1% NP-40). After antibody binding, the mixture was added to the washed beads and gently mixed, followed by incubation for 1 hour at 4°C with rotation. After incubation, the RNA-bound beads were washed four times with 700 µL beads wash buffer 2 (RNase-free water containing 350 mM KCl, 5 mM $MgCl_2$, 10 mM HEPES [pH 7.4], 1% NP-40, 2 mM DTT, 100 U/mL recombinant RNasin (Promega), 100 µg/mL cycloheximide, 5 mM sodium fluoride, 1 mM sodium orthovanadate, 1 mM sodium pyrophosphate, 1 mM beta-glycerophosphate). During the final wash, beads were placed onto the magnet and moved to room temperature. After removing supernatant, RNA was eluted by mixing the beads with 350 µL RLT (Qiagen). The eluted RNA was purified using RNeasy Micro kit (Qiagen). Chemicals were purchased from Sigma if not specified otherwise.

cDNA from purified RNA were generated using SMART-Seq v4 Ultra Low Input RNA Kit (Takara Clontech). Libraries were made using the Nexterra XT DNA Library Preparation Kit. Up to 12 samples were pooled and sequenced on Illumina HiSeq2000/2500 on single-

end read mode. RNA-Seq data was aligned using Kallisto. Differential expression analysis was performed using a combination of DESeq and EdgeR packages in R.

## Open-field behavior test

The behavior of the mice was observed on post-surgery 1 and 3 day. Three groups of mice were observed, *i.e.*, no-injury control, olive oil control, and BCP groups. The no-injury control group had the dorsal hair removed and a bandage placed on the day when other mice went through surgeries, but no incision was made. Bandages of these mice were changed daily as well. The olive oil control and BCP groups underwent the procedure detailed above. A mouse was placed in a cup (about 10 cm diameter x 15 cm height) and placed in the center of an open field test apparatus (measurements: width 50 cm x depth 25 cm x height 30 cm) covered with the cup. Video recording using a camera (Logitech QuickCam Pro9000) and bTV software was conducted either from the top for analysis of the amount of traveling or from the side for analysis of behavior patterns. After camera was started, the cup covering the mouse was removed and behaviors were recorded for 5 minutes. The behaviors recorded from the top were analyzed using Ethovision (Version 7, Noldus, Leesburg, VA) and behaviors recorded from the side were analyzed using ELAN software (http://tla.mpi.nl/tools/tla-tools/elan/, Max Planck Institute for Psycholinguistics, The Language Archive, Nijmegen, The Netherlands) [76]. Behaviors were categorized based on the definition given by [77-79] and quantified using ELAN software. The behaviors coded for using ELAN were then exported to Microsoft Excel where average time for each behavior, incidence of each behavior, and total time for each behavior were determined.

## Statistical analyses

ANOVA and Student T-tests were used for comparison of the groups. Tukey post-hoc test was used for pair-wise comparison. Comparison of % was conducted using Fisher's exact test of indepence.

**Acknowledgements**

This project was funded by the Office of the Vice Provost of Research at Indiana University Bloomington through the Collaborative Research and Creative Activity Funding Award to S.K. while she was Associate Research Professor at the Medical Science Program of the School of Medicine of IU. Large amount of this project was conducted while S.K. was Associate Research Professor at the Medical Science Program of the School of Medicine of IU, financially supported by the previous Director of Medical Science Program, Prof. John Watkins III. S.K thanks A. Straiker of the Department of Psychological and Brain Sciences, IU, for his kind gift of CB2 agonist and antagonist used in the project and also for the advice on CB2. S.K thanks J. Wager-Miller of the Department of Psychological and Brain Sciences, IU, for his kind gift of CB2 knockout mice in the project. S.K. thanks J. Foley of Medical Science Program of IU School of Medicine to let S.K. use part of his laboratory space and resources for the project. S.K. thanks S. Childless of Medical Science Program of IU School of Medicine for her help in sectioning samples and J.K. Leffel II of Department of Psychological and Brain Sciences, IU, for his help on using Ethovision. RNA sequencing and bioinformatic analyses was conducted at the Center for Genomics and Bioinformatics of IUB and S.K. thanks A.M. Buechlein, D.B. Rusch and J. Huang for their services. S.K. also thanks K. Mackie

of the Department of Psychological and Brain Sciences for his advice on the project, J. Powers of the IU Light Microscopy Imaging Center (LMIC) for his help and advice while using LMIC, and D. Sinkiewicz of the Center for the Integrative Study of Animal Behavior Laboratory (CISAB Lab) for advice. S.K. thanks the staff of laboratory animal resources (LAR) of IU for their assistance in maintaining her mice colony.

# References

1. Koyama S. Primer Effects by Murine Pheromone Signaling. Pheromonal Influences on Reproductive Conditions. Springer International Publishing AG, Vienna: Springer Briefs in Animal Sciences, Springer; 2016.
2. Kim JT, Ren CJ, Fielding GA, Pitti A, Kasumi T, Wajda M, Lebovits A, Bekker A. Treatment with lavender aromatherapy in the post-anesthesia care unitreduces opioid requirements of morbidly obese patients undergoing laparoscopic adjustable gastric banding. Obes Surg. 2007;17(7): 920-925.
3. Marzouk T, Barakat R, Ragab A, Badria F, Badawy A. Lavender-thymol as a new topical aromatherapy preparation for episiotomy: a randomized clinical trial. J Obstet Gynaecol. 2015;35(5): 472-475.
4. Malcolm BJ, Tallian K. Essential oil of lavender in anxiety disorders: ready for prime time? Ment Health Clin. 2017;7(4): 147-155.
5. Nasiri A, Mahmodi MA. Aromatherapy massage with lavender essential oil and the prevention of disability in ADL in patients with osteoarthritis of the knee: a randomized controlled clinical trial. Complement Ther Clin Pract. 2018;30: 116-121.

6. Schneider R, Singer N, Singer T. Medical aromatherapy revisited- basic mechanisms, critique, and a new development. Hum Psychopharmacol Clin Exp. 2019;34: e2683.
7. Kang N, Koo J. Olfactory receptors in non-chemosensory tissues. BMB Rep. 2012;45(11): 612-622.
8. Chen Z, Zhao H, Fu N, Chen L. The diversified function and potential therapy of ectopic olfactory receptors in non-olfactory tissues. J Cell Physiol. 2018;233(3): 2104-2115.
9. Gertsch J, Leonti M, Raduner S, Racz I, Chen JZ, Xie XQ, Altmann K-H, Karsak M, Zimmer A. Beta-caryophyllene is a dietary cannabinoid. Proc Natl Acad Sci USA. 2008;105: 9099-9104.
10. Zheng JL, Yu TS, Li XN, Fan YY, Ma WX, Du Y, Zhao R, Guan D-W. Cannabinoid receptor type 2 is time-dependently expressed during skin wound healing in mice. Int J Legal Med. 2012;126(5): 807-814.
11. Li SS, Wang LL, Liu M, Jiang SK, Zhang M, Tian ZL, Wang M, Li J-Y, Zhao R, Guan D-W. Cannabinoid CB2 receptors are involved in the regulation of fibrogenesis during skin repair in mice. Mol Med Rep. 2016;13(4): 3441-3450.
12. Wang LL, Zhao R, Li JY, Liu M, Wang M, Zhang MZ, Dong W-W, Jiang S-K, Xhang M, Tian Z-L, Liu C-S, Guan D-W. Pharmacological activation of cannabinoid 2 receptor attenuates inflammation, fibrogenesis and promotes re-epithelialization during skin wound healing. Eur J Pharmacol. 2016;786: 128-136.
13. Amorim JL, Figueiredo JB, Amaral ACF, Barros EGO, Pelmero C, MPalantinos MA, Ramos AdS, Ferreira JLP, Silva JRdA, Benjamim CF, Basso SL, Nasciutti LE, Fernandes

PD. Wound healing properties of *Copaifera paupera* in diabetic mice. PloS One. 2017;12(10): e0187380.

14. Gonzalez AC, Costa TF, Andrade ZA, Medrado AR. Wound healing – A literature review. An Bras Dermatol. 2016;91(5): 614-620.
15. Landen NX, Li D, Stahle M. Transition from inflammation to proliferation: a critical step during wound healing. Cell Mol Life Sci. 2016;73: 3861-3885.
16. Rittie L. Cellular mechanisms of skin repair in humans and other animals. J Cell Commun Signal. 2016;10: 103-120.
17. Sorg H, Tilkorn DJ, Hager S, Hauser J. Skin wound healing: an update on current knowledge and concepts. Eur Surg Res. 2017;58(1-2): 81-94.
18. Braiman-Wiksman L, Solomonik I, Spira R, Tennenbaum T. Novel insights into wound healing sequence of events. Toxicol Pathol. 2007; 35: 767-779.
19. Tracy LE, Minasian RA, Caterson EJ. Extracellular matrix and dermal fibroblast function in the healing wound. Adv Wound Care (New Rochelle). 2016; 5(3): 119-136.
20. Kezic S, Jakasa I. Filaggrin and skin barrier function. Curr Probl Dermatol. 2016; 49: 1-7.
21. Ashcroft GS, Dodsworth J, van Boxtel E, Tarnuzzer RW, Horan MA, Schultz GS, Ferguson MWJ. Estrogen accelerates cutaneous wound healing associated with an increase in TGF-beta1 levels. Nat Med. 1997;3(11): 1209-1215.
22. Heldin CH, Westermark B. Mechanism of action and in vivo role of platelet-derived growth factor. Physiol Rev. 1999; 79(4): 1283-1316.

23. Horikawa S, Ishii Y, Hamashima T, Yamamoto S, Mori H, Fujimori T, Shen J, Inoue R, Nishizono H, Itoh H, Majima M, Abraham D, Miyawaki T, Sasahara M. PDGFRα plays a crucial role in connective tissue remodeling. Sci Rep. 2016; 5:17948. Doi: 10.1038/Srep17948.

24. Ivaska J, Pallari HM, Nevo J, Eriksson JE. Novel functions of vimentin in cell adhesion, migration, and signaling. Exp Cell Res. 2007; 313(10): 2050-2062.

25. Cheng F, Shen Y, Mohanasundaram P, Lindstrom M, Ivaska J, Ny T, Eriksson JE. Vimentin coordinates fibroblast proliferation and keratinocyte differentiation in wound healing via TGF-β-slug signaling. Proc Natl Acad Sci U S A. 2016; 113(30): E4320-4327.

26. Solanas, G., Benitah, S.A. Regenerating the skin: a task for the heterogeneous stem cell pool and surrounding niche. Nat Rev Mol Cell Biol 2013; 14: 737-748.

27. Kretzschmar, K., Watt, F.M. Markers of epidermal stem cell subpopulations in adult mammalian skin. Cold Spring Harb Perspect Med 2014; 4: a013631.

28. Watt, F.M. Mammalian skin cell biology: At the interface between laboratory and clinic. Science 2014; 346: 937-940.

29. Aragona M, Dekoninck S, Rulands S, Lenglez S, Mascre G, Simons BD, Blanpain C. Defining stem cell dynamics and migration during wound healing in mouse skin epidermis. Nat Comm. 2017;8: Article number 14684.

30. Ito, M., Liu, Y., Yang, Z., Nguyen, J., Liang, F., Morris, R.J., Cotsarelis, G. Stem cells in the hair follicle bulge contribute to repair but not to homeostasis of epidermis. Nat Med 2005; 11: 1351-1354.

31. Pertwee R, Griffin G, Fernando S, Li X, Hill A, Makriyannis A. AM630, a competitive cannabinoid receptor antagonist. Life Sci. 1995; 56(23-24): 1949-1955.

32. Huffman, JW. CB2 receptor ligands. Mini Rev Med Chem. 2005; 5(7): 641-649.

33. Wu DD, Inwin DM, Zhang YP. Molecular evolution of the keratin associated protein gene family in mammals, role in the evolution of mammalian hair. BMC Evol Biol. 2008; 8: 241. Doi: 10.1186/1471-2148-8-241.

34. Fujikawa H, Fujimoto A, Farooq M, Ito N, Shimomura Y. Characterization of the human hair keratin-associated protein 2 (KRTAP2) gene family. J Invest Dermatol. 2012;132: 1806-1813

35. Kuno K, Kanada N, Nakashima E, Fujiki F, Ichimura F, Matsushima K. Molecular cloning of a gene encoding a new type of metalloproteinase-disintegrin family protein with thrombospondin motifs as an inflammation associated gene. J Biol Chem. 1997; 272(1): 556-562.

36. Grotewold L, Plum M, Dildrop R, Peters T, Ruther U. Bambi is coexpressed with Bmp-4 during mouse embryogenesis. Mech Dev. 2001; 100(2): 327-330.

37. Liu YH, Ma L, Wu LY, Luo W, Kundu R, Sangiorgi F, Snead ML, Maxson R. Regulation of the Msx2 homeobox gene during mouse embryogenesis: a transgene with 439 bp of 5' flanking sequence is expressed exclusively in the apical ectodermal ridge of the developing limb. Mech Dev. 1994; 48(3): 187-197.

38. Morasso MI, Markova NG, Sargent TD. Regulation of epidermal differentiation by a Distal-less homeodomain gene. J Cell Biol. 1996; 135(6 Pt 2): 1879-1887.

39. Dong S, Yng S, Kojima T, Shiraiwa M, Kawada A, Mechin MC, Adoue V, Chavanas S, Serre G, Simon M, Takahara H. Crucial roles of MZF1 and Sp1 in the transcriptional

regulation of the peptidylarginine deiminase type I gene (PADI1) in human keratinocytes. J Invet Dermatol. 2008; 128(3): 549-557.

40. Jave-Suarez LF, Winter H, Langbein L, Rogers MA, Schweizer J. HOXC13 is involved in the regulation of human hair keratin gene expression. J Biol Chem. 2002; 277(5): 3718-3726.
41. Breen EC, Tang K. Calcyclin (S100A6) regulates pulmonary fibroblast proliferation, morphology, and cytoskeletal organization in vitro. J Cell Biochem. 2003; 88(4): 848-854.
42. Kondo T, Ohshima T. The dynamics of inflammatory cytokines in the healing process of mouse skin wound: a preliminary study for possible wound age determination. Int J Legal Med. 1996; 108: 231-236.
43. St Laurent G III, Seilheimer B, Tackett M, Zhou J, Shtokalo D. Vyatkin Y, Ri M, Toma I, Jones D, McCaffrey TA. Deep sequencing transcriptome analysis of murine wound healing: effects of a multicomponent, multitarget natural product therapy-Tr14. Front Mol Biosci. 2017;17: https://doi.org/10.3389/fmolb.2017.00057.
44. Premkumar LS. Transient receptor potential channels as targets for phytochemicals. ACS Chem Neurosci. 2014; 5(11): 1117-1130.
45. Caterina MJ. TRP channel cannabinoid receptors in skin sensation, homeostasis, and inflammation. ACS Chem Neurosci. 2014; 5(11): 1107-1116.
46. Premkumar LS, Abooj M. TRP channels and analgesia. Life Sci. 2013; 92(8-9): 415-424.

47. Colonna M, Facchetti F. TREM-1 (triggering receptor expressed on myeloid cells): a new player in acute inflammatory responses. J Infect Dis. 2003; 187 Suppl 2: S397-401.

48. Johnson RL, Riddle RD, Laufer E, Tabin C. Sonic hedgehog: a key mediator of anterior-posterior patterning of the limb and dorso-ventral patterning of axial embryonic structures. Biochem Soc Trans. 1994; 22(3): 569-574.

49. Eaton S. Planar polarization of drosophila and vertebrate epithelia. Curr Opin Cell Biol. 1997; 9(6): 880-886.

50. Maddaluno L, Urwyler C, Werner S. Fibroblast growth factors: key players in regeneration and tissue repair. Development, 2017; 144(22): 4047-4060.

51. MacDonald BT, Tamai K, He X. Wnt/beta-catenin signaling: components, mechanisms, and diseases. Dev Cell. 2009; 17(1): 9-26.

52. Abe, Y., Tanaka, N. Roles of hedgehog signaling pathway in epidermal and hair follicle development, homeostasis, and cancer. J Dev Biol 2017; 5: E12 doi: 10.3390/jdb5040012.

53. Brownell, I. Guevara, E., Bai, C.B., Loomis, C.A., Joyner, A.L. Nerve-derived sonic hedgehog defines a niche for hair follicle stem cells capable of becoming epidermal stem cells. Cell Stem Cell 2011; 8(5): 552-565.

54. Caddy, J., Wilanowski, T., Darido, C., Dworkin, S., Ting, S.B. Zhao Q, Rank G, Auden A, Srivastava S, Papenfuss TA, Murdoch JN, Humbert PO, Boulos N, Weber T, Zuo J, Cunningham JM, Jane SM. Epidermal wound repair is regulated by the planar cell polarity signaling pathway. Dev Cell 2010; 19(1): 138-147.

55. Bayly, R., Axelrod, J.D. Pointing in the right direction: new developments in the field of planar cell polarity. Nat Rev Genet 2011; 12(6): 385-391.

56. Munoz-Soriano, V., Belacortu, Y., Paricio, N. Planar cell polarity signaling in collective cell movements during morphogenesis and disease. Curr Genomics 2012; 13(8): 609-622.

57. Richardson, R., Metzger, M., Knyphausen, P., Ramezani, T., Slanchev, K., Kraus, C., Schmelzer, E., Hammerschmidt, M. Re-epithelialization of cutaneous wounds in adult zebrafish combines mechenisms of wound closure in embryonic and adult mammals. Development 2016; 143: 2077-2088.

58. Azzi L, El-Alfy M, Martel C, Labrie F. Gender differences in mouse skin morphology and specific effects of sex steroids and dehydroepiandrosterone. J. Invest. Dermatol. 2005;124(1): 22-27.

59. Ashcroft GS, Mills SJ. Androgen receptor-mediated inhibition of cutaneous wound healing. J Clin Invest. 2002;110(5), 615-624.

60. Gilliver SC, Ashcroft GS. Sex steroids and cutaneous wound healing: the contrasting influences of estrogens and androgens. Climacteric. 2007;10(4) 276-288.

61. Busse D, Kudella P, Gruening NM, Gisselmann G, Stander S, Luger T, Jacobsen F, Steinstrasser L, Paus R, Gkogkolou P, Bohm M, Hatt H, Benecke H. A synthetic sandalwood odorant induces wound-healing processes in human keratinocytes via the olfactory receptor OR2AT4. J Invest Dermatol. 2014;134(11): 2823-2832.

62. Harada H, Kashiwadani H, Kanmura Y, Kuwaki T. Linalool odor-induced anxiolytic effects in mice. Front Behav Neurosci. 2018;12: 241 doi: 10.3389/fnbeh.2018.00241.

63. Jiang Y, Gong NN, Hu XS, Ni MJ, Pasi R, Matsunami H. Molecular profiling of activated olfactory neurons identifies odorant receptors for odors *in vivo*. Nat Neurosci. 2015;18: 1446-1454.

64. Sicard G, Holley A. Receptor cell responses to odorants: similarities and differences among odorants. Brain Res. 1985;292: 283-296.

65. Fleischer J, Breer H, Strotmann J. Mammalian olfactory receptors. Front Cell Neurosci. 2009;3: 9. Doi: 10.3389/neuro.03.009.2009.

66. Mahmoud MF, Swefy SE, Hasan RA, Ibrahim A. Role of cannabinoid receptors in hepatic fibrosis and apoptosis associated with bile duct ligation in rats. Eur J Pharmacol. 2014;742: 118-124.

67. Yang M, Lv Y, Tian X, Lou J, An R, Zhang Q, Li M, Dong Z. Neuroprotective effect of β-caryophyllene on cerebral ischemia-reperfusion injury via regulation of necroptotic neuronal death and inflammation: In vivo and in vitro. Front. Neurosci. 2017;11: 583.

68. Fuchs, Y., Brown, S., Gorenc, T., Rodriguez, J., Fuchs, E., Steller, H. *Sept4*/ARTS regulates stem cell apoptosis and skin regeneration. Science 2013; 341: 286-289.

69. Wilgus TA, Bergdall VK, DiPietro LA, Oberyszyn TM. Hydrogen peroxide disrupts scarless fetal wound repair. Wound Repair Regen. 2005;13(5): 513-519.

70. Mescher AL. Macrophages and fibroblasts during inflammation and tissue repair in models of organ regeneration. Regeneration. 2017;4: 39-53.

71. Vanderhaeghen P, Schurmans S, Vassart G, Parmentier M. Olfactory receptors are displayed on dog mature sperm cells. J Cell Biol. 1993;123(6 Pt1): 1441-1452.

72. Vosshall LB. Olfaction: attracting both sperm and the nose. Curr Biol. 2004;14(21): R918-920.

73. Adams RP. Identification of essential oil components by gas chromatography/ quadrupole mass spectroscopy. Carol Streams: Allured Publishing Corporation; 2001.

74. Jemiolo B, Harvey S, Novotny M. Promotion of the Whitten effect in female mice by synthetic analogs of male urinary constituents. Proc Natl Acad Sci USA. 1986;83(12): 4576-4579.

75. Harvey S, Jemiolo B, Novotny M. Pattern of volatile compounds in dominant and subordinate male urine. J Chem Ecol. 1989;15(7): 2061-2072.

76. Lausberg H, Sloetjes H. Coding gestural behavior with NEUROGES—ELAN system. Behav Res Methods. 2009;41(3): 841-849.

77. Grant EG, Mackintosh JH. A comparison of the social posture of common laboratory rodents. Behaviour, 1963;21: 247-259.

78. Wilson RC, Vacek T, Lanier DL, Dewsbury DA. Open-field behavior in muroid rodents. Behav Biol. 1976;17: 495-506.

79. Weyers P, Janke W, Macht M, Weijers HG. Social and non-social open field behaviours of rats under light and noise stimulation. Behav Processes. 1994;31: 257-268.

80. Sköld M, Karlberg AT, Matura M, Börje A. The fragrance chemical beta-caryophyllene-air oxidation and skin sensitization. Food Chem Toxicol. 2005;44: 538-545.

81. Kalueff AV, Tuohimaa P. Grooming analysis algorithm for neurobehavioural stress research. Brain Res Brain Res Protoc. 2004;13(3): 151-158.

82. Smolinsky AN, Bergner CL, LaPorte JL, Kalueff AV. Analysis of grooming behavior and its utility in studying animal stress, anxiety, and depression . In: Gould TD, editor. Mood and Anxiety Related Phenotypes in Mice, Neuromethods 2017,42, DOI 10.1007/978-1-60761-303-9_2, © Humana Press.

**Author contributions:** S.K conceptualized and led the study. S.K., A.P., and M.K. performed the *in vivo* mouse experiments. S.K. performed all the *in vitro* assays. H.M. conducted pS6-IP RNA-Seq experiments. A.M. analyzed the results of RNA sequencing, read the manuscript, and discussed with S.K. while finalizing it as a paper. K.D. and C.K. edited the manuscript and provided important comments on the organization and experimental approaches. H.A.S. and M.V.N. prepared SBT solution and analyzed the BCP from Sigma-Aldrich, read and edited the manuscript. S.K. wrote the manuscript with input from other authors.

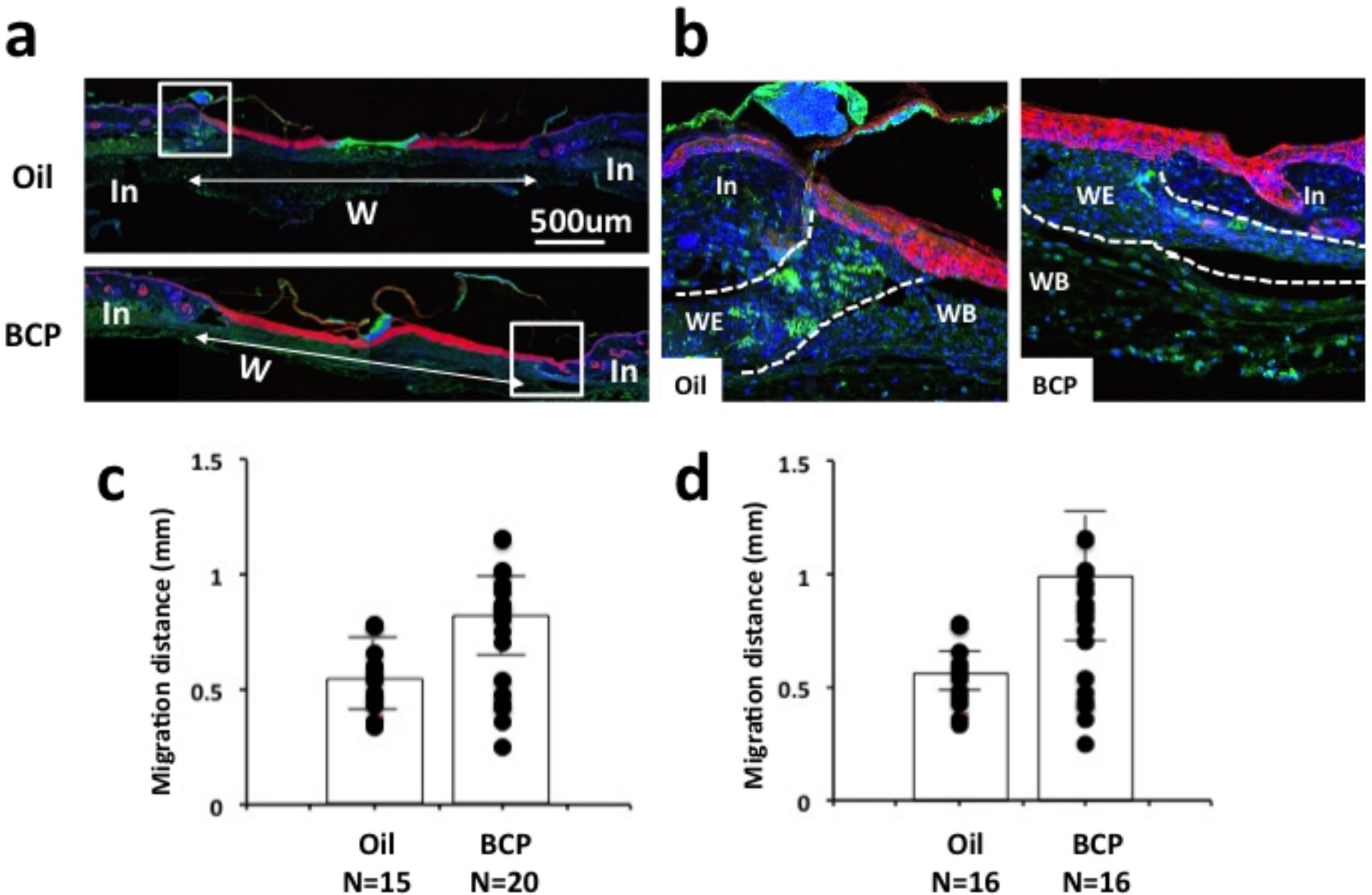
a
Oil
In
In
W
500um
BCP
In
W
In
b
In
WE
WB
Oil
WE
In
WB
BCP
c
Migration distance (mm)
1.5
1
0.5
0
Oil
N=15
BCP
N=20
d
Migration distance (mm)
1.5
1
0.5
0
Oil
N=16
BCP
N=16

Figure1

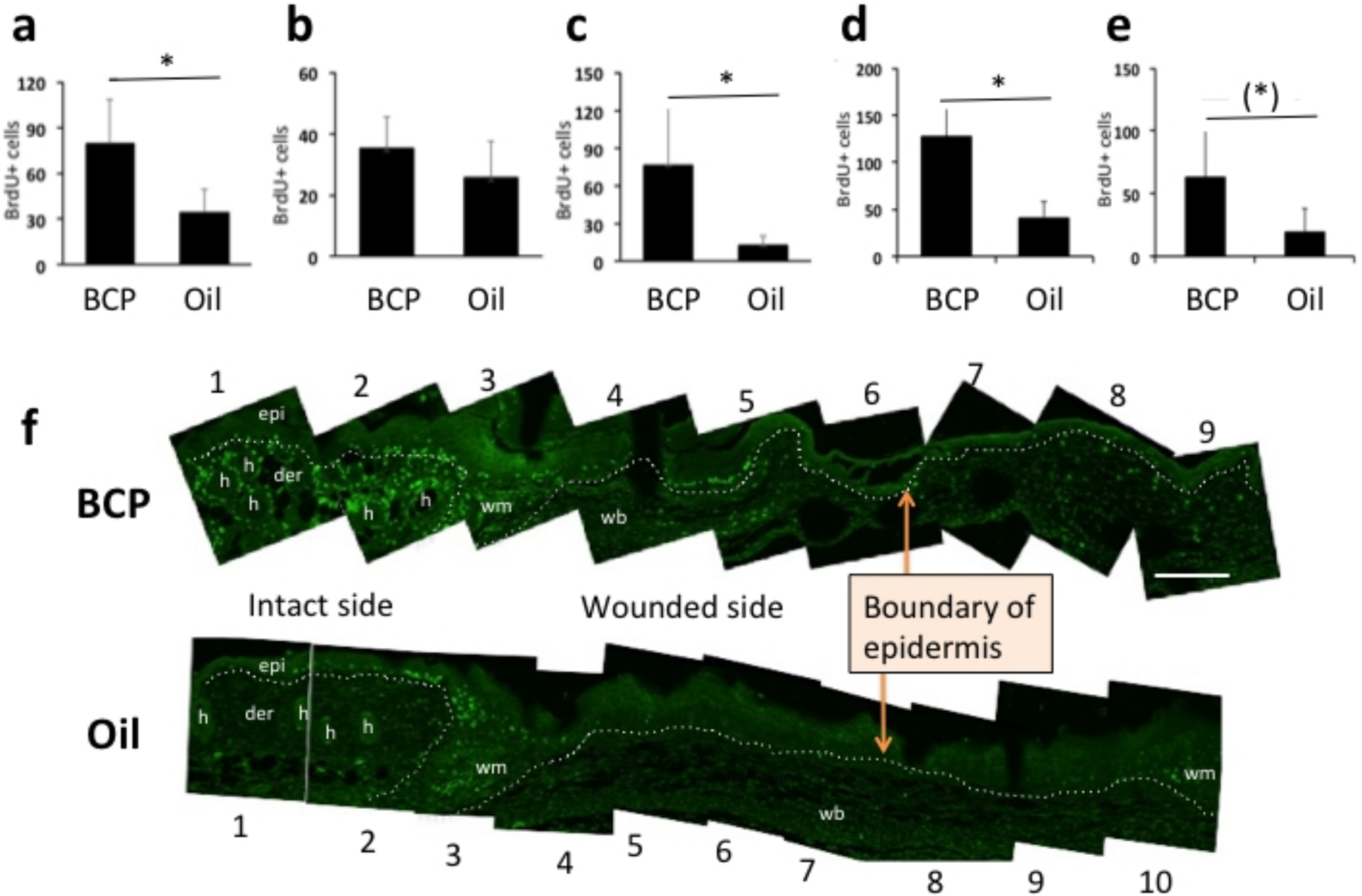
a
b
c
d
e
BrdU+ cells
*
(*)
BCP
Oil
f
BCP
Oil
epi
der
h
wm
wb
1
2
3
4
5
6
7
8
9
10
Intact side
Wounded side
Boundary of epidermis

Figure3

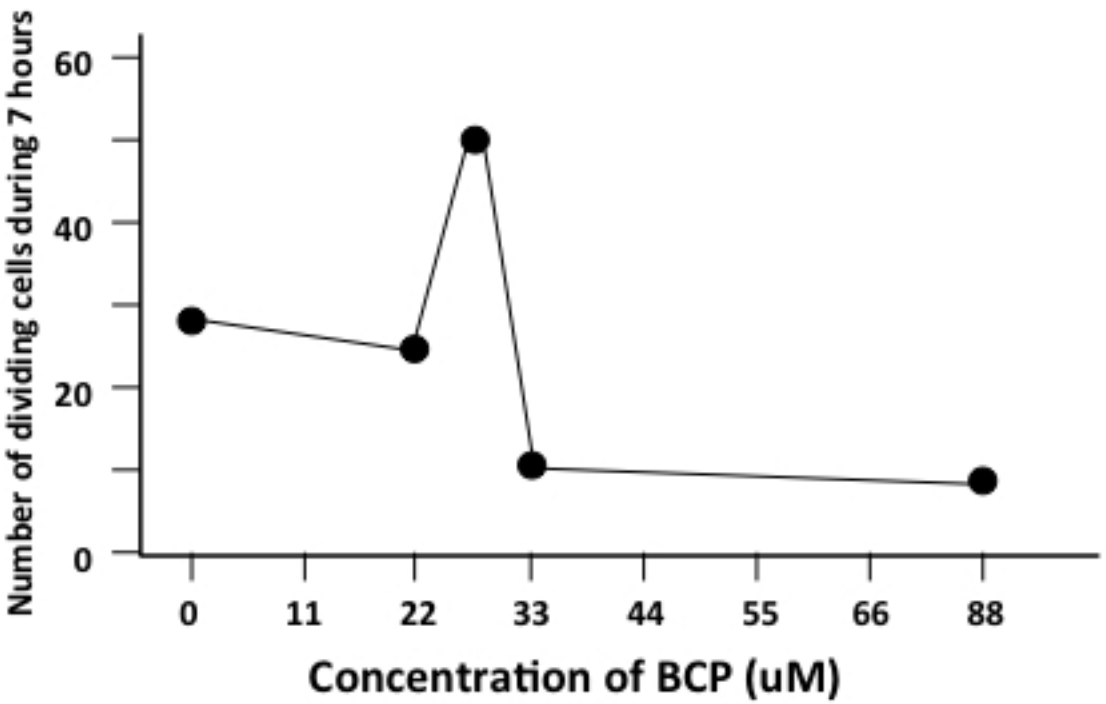
Number of dividing cells during 7 hours
60
40
20
0
0
11
22
33
44
55
66
88
Concentration of BCP (uM)

Figure4

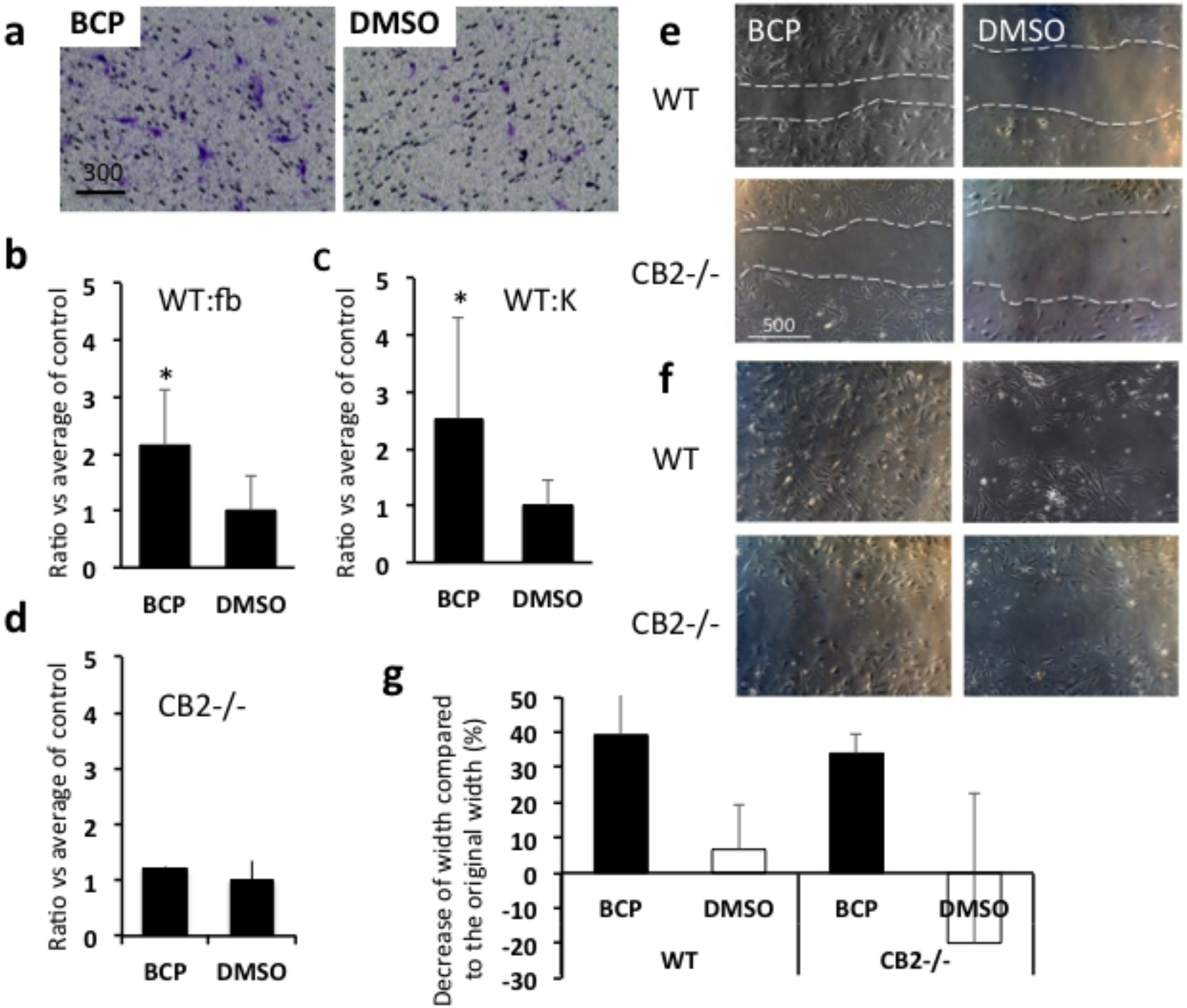
a
BCP
DMSO
300
b
WT:fb
Ratio vs average of control
BCP
DMSO
c
WT:K
Ratio vs average of control
BCP
DMSO
d
CB2-/-
Ratio vs average of control
BCP
DMSO
e
BCP
DMSO
WT
CB2-/-
500
f
WT
CB2-/-
g
Decrease of width compared to the original width (%)
BCP
DMSO
BCP
DMSO
WT
CB2-/-

Figure5

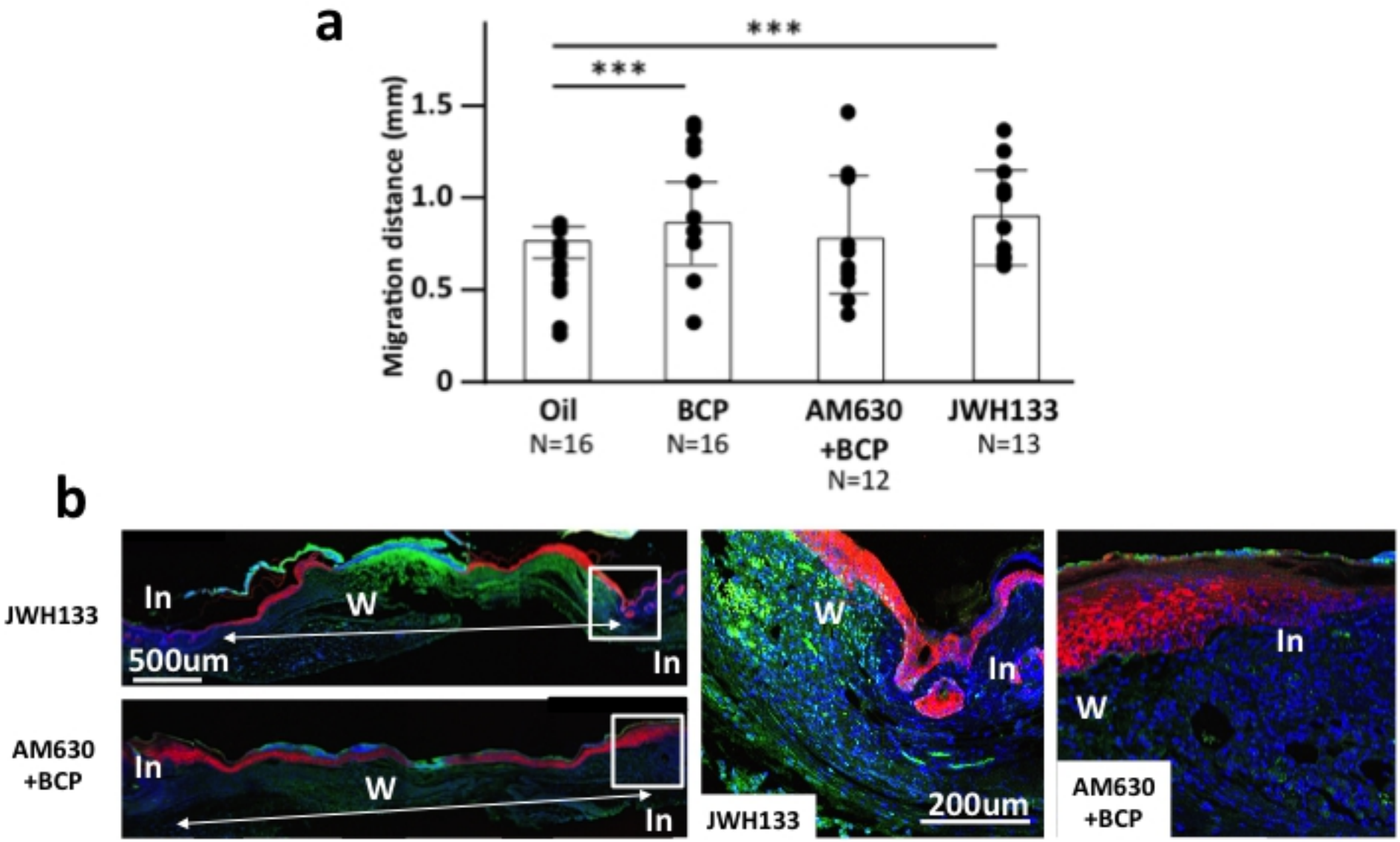
a
***
***
Migration distance (mm)
1.5
1.0
0.5
0
Oil
N=16
BCP
N=16
AM630
+BCP
N=12
JWH133
N=13
b
JWH133
AM630
+BCP
In
W
500um
In
In
W
In
W
In
In
W
200um
JWH133
In
W
AM630
+BCP

Figure6

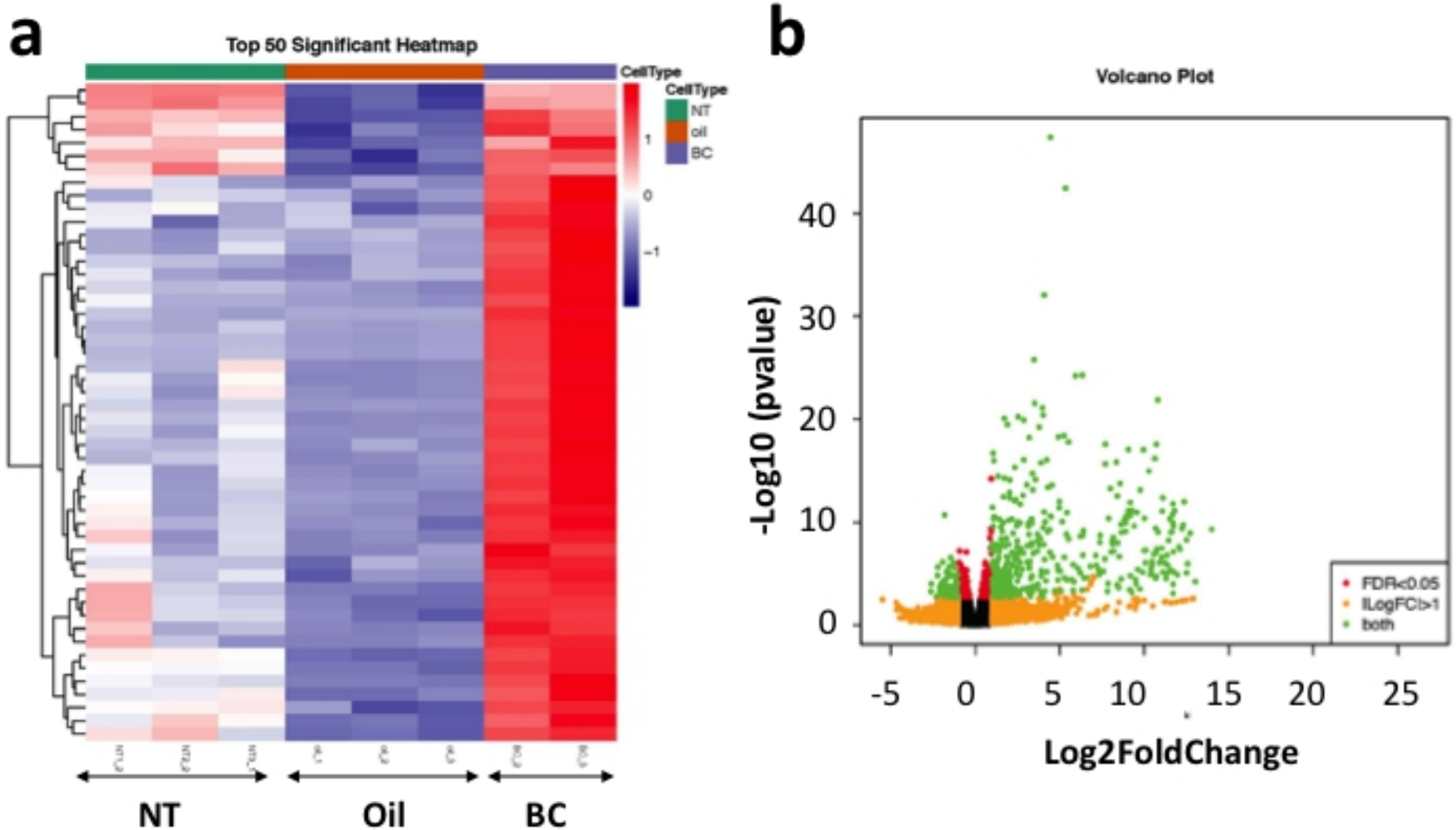
a
Top 50 Significant Heatmap
CellType
NT
oil
BC
1
0
−1
NT
Oil
BC
b
Volcano Plot
-Log10 (pvalue)
40
30
20
10
0
-5
0
5
10
15
20
25
Log2FoldChange
FDR<0.05
|LogFC|>1
both

Figure7

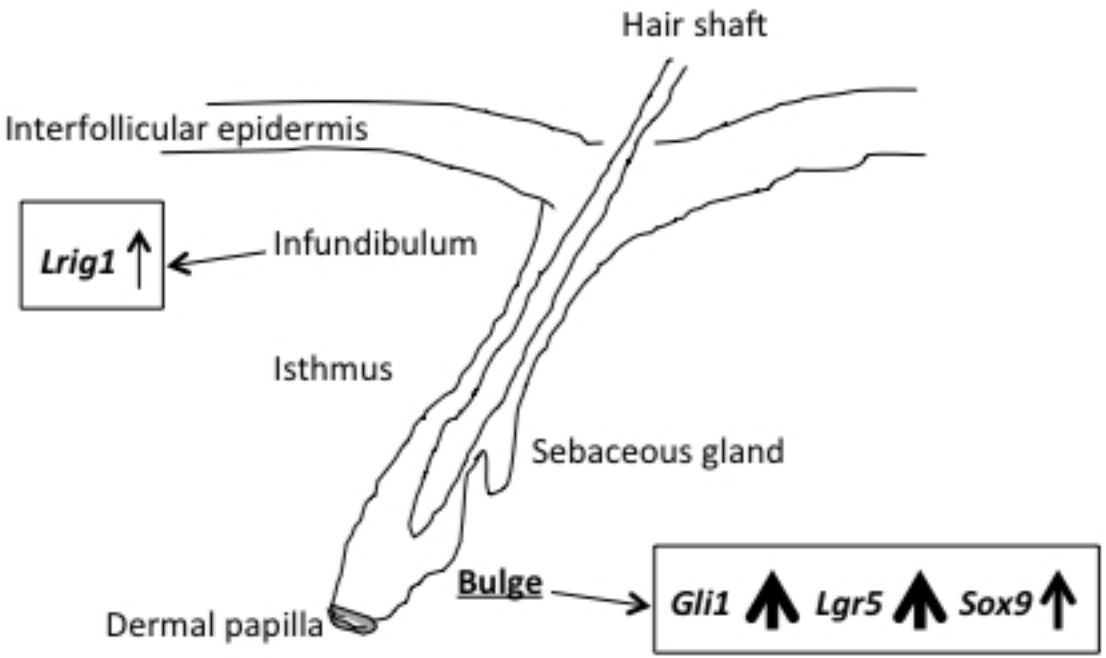


Expression of epidermal stem cell markers

| Location | Gene | Logfoldchange | Pvalue | |
|---|---|---|---|---|
| interfollicular epidermis | *Lgr6* | 0.384 | 0.08 | |
| hair follicle Infundibulum | *Lrig1* | 0.4035 | 0.013 | * |
| | *Plet1* | -0.283 | 0.172 | |
| isthmus | *Lgr6* | 0.384 | 0.08 | |
| bulge | *Gli1* | 2.4605 | 1.76E-07 | *** |
| | *Lgr5* | 1.236 | 0.001 | *** |
| | *CD34* | -0.199 | 0.454 | |
| | *Krt15* | 0.0646 | 0.71 | |
| | *Krt19* | 0.456 | 0.298 | |
| | *Sox9* | 0.5377 | 0.003 | ** |
| sebaceous gland duct | *Blimp1 (Prdu1)* | 0.3291 | 0.081 | |

Figure8

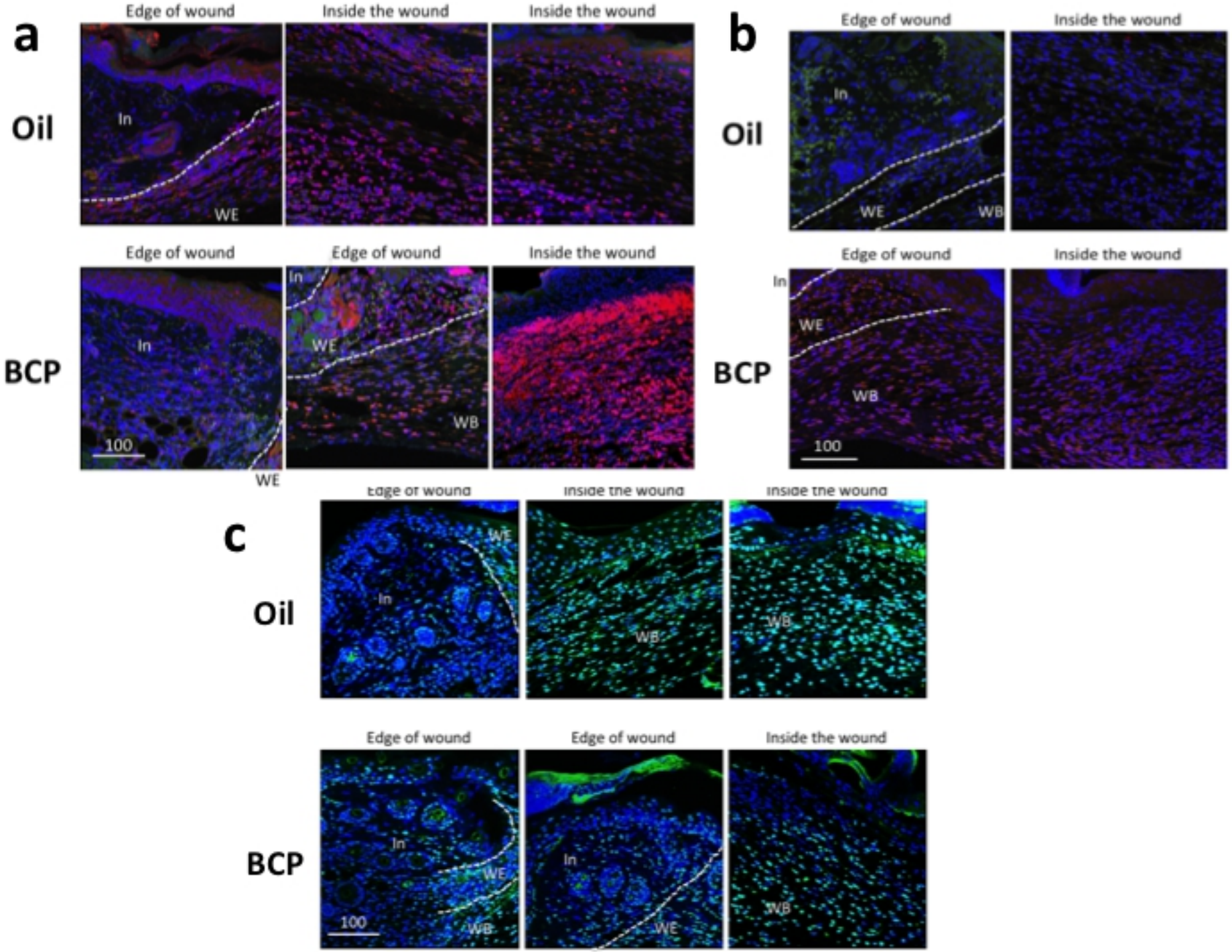
a
Oil
Edge of wound
Inside the wound
Inside the wound
In
WE
BCP
Edge of wound
Edge of wound
Inside the wound
In
WE
WB
100
b
Oil
Edge of wound
Inside the wound
In
WE
WB
BCP
Edge of wound
Inside the wound
In
WE
WB
100
c
Oil
Edge of wound
Inside the wound
Inside the wound
WE
In
WB
BCP
Edge of wound
Edge of wound
Inside the wound
In
WE
WB
100

Figure9

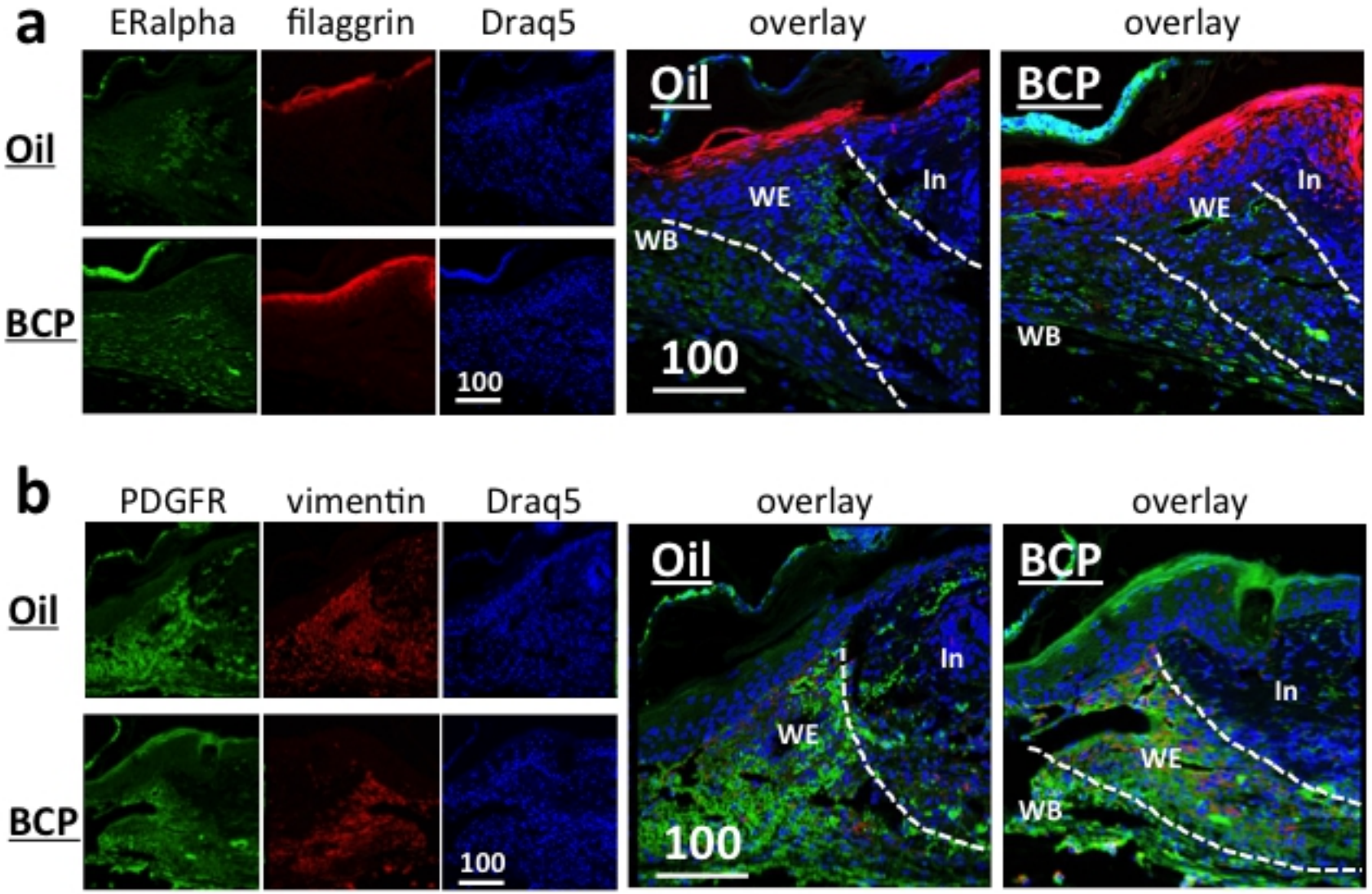
a
ERalpha
filaggrin
Draq5
overlay
overlay
Oil
BCP
Oil
BCP
WE
In
WB
100
b
PDGFR
vimentin
Draq5
overlay
overlay
Oil
BCP
Oil
BCP
WE
In
WB
100

Figure2

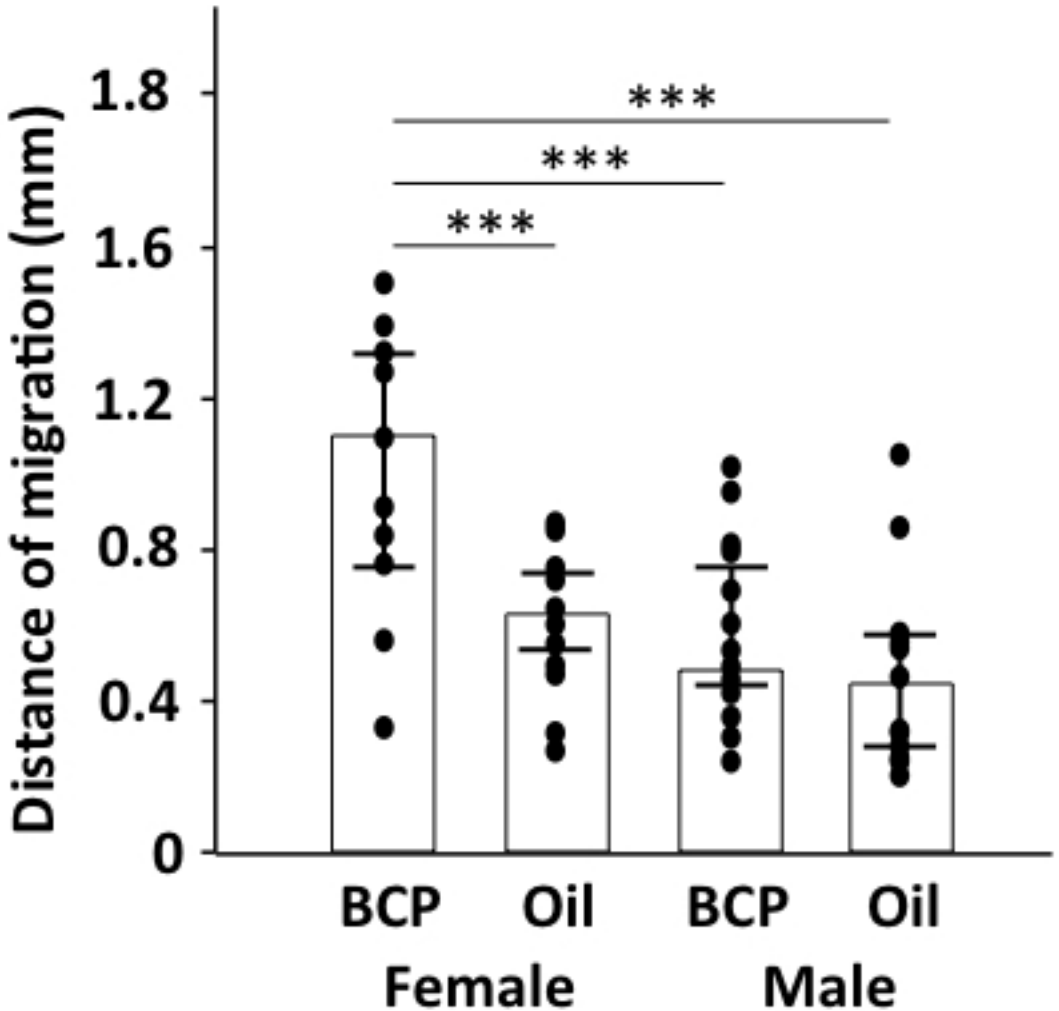
Distance of migration (mm)
1.8
1.6
1.2
0.8
0.4
0
***
***
***
BCP
Oil
BCP
Oil
Female
Male

Figure10